INVESTIGATION OF IMPURITY RADIATION FROM A WELL DIAGNOSED, LASER HEATED PLASMA SAMPLE

FINAL REPORT

LAWRENCE LIVERMORE LABORATORY
Livermore, CA

MN ONLY

By

E. Crawford
D. Quimby
A. Hoffman
Z.A. Pietrzyk

Submitted

November 1, 1977

MATHEMATICAL SCIENCES NORTHWEST, INC.
P. O. Box 1887
Bellevue, Washington 98009

TABLE OF CONTENTS

LIST OF TABLES

LIST OF FIGURES

SECTION I

INTRODUCTION

This report describes the results of an experimental and theoretical program designed to measure the relative intensities of line radiation from various ionization stages of carbon and helium impurities added to a deuterium plasma, and to relate the observed line intensity ratios to the plasma temperature. Using the facility and methodology discussed in detail in MSNW Report 77-1058-1, a deuterium sample plasma is produced and heated to a temperature of 2 to 7 eV at an electron density of 5×10^{16} cm^{-3}. The plasma parameters are monitored at various discrete times during the plasma decay using the Thomson scattering system described in Reference 1. Simultaneously, the same sample volume is observed in the visible region of the spectrum using a streak camera coupled to a spectrograph. A continuous record of the plasma visible spectrum is thus obtained during the plasma time history, with at one specific time a data point on the plasma parameters, n_e and T_e.

Modifications were made to the plasma sample facility to shorten the duration of the preionization current and to increase its magnitude. This modification accomplished the desired effect of increasing the electron density in the heated plasma to 5×10^{16}, essentially obtaining full filling density. Additional insulation was added to the solenoid and satisfactory simultaneous operation of the solenoid at a 20 kV charging voltage and the preionization discharge at a 40 kV charging voltage was demonstrated.

A series of Thomson scattering experiments, with simultaneous spectroscopy have essentially reproduced the results, and plasma conditions obtained in Reference 1, and the resulting hard film spectra have been sent to LLL for processing and preliminary data analysis.

SECTION II

MODIFICATIONS TO PLASMA SAMPLE FACILITY

Several modifications to the plasma sample facility were made to improve the preionization condition, to allow operation at higher field strengths for improved magnetic insulation, and to improve optical access to the sample volume.

1. Varistor Damping of Preionization Discharge

The preionization discharge capacitor bank was completely rebuilt, since the ignitron switched device with linear resistance damping described in Ref. 1 was unsatisfactory in several respects. A pressurized spark gap switch of MSNW design was installed, and a PATT55 spiral generator was used as a trigger device. A non-linear damping system consisting of three type 68W60100 (MCI) varistors connected in series with the capacitor and switch was added. This arrangement performed as expected, producing a 20 kA peak preionization current in approximately 350 nsec when used with an 0.25 μf capacitor charged to 40 kV. Figure 1 shows the waveform calculated for this device (see Section IV) with several points measured from an experimental waveform plotted on it for comparison.

2. Solenoid Insulation

Additional insulation was added to the solenoid as shown in Figure 2. This prevented breakdown from the solenoid to the Z discharge

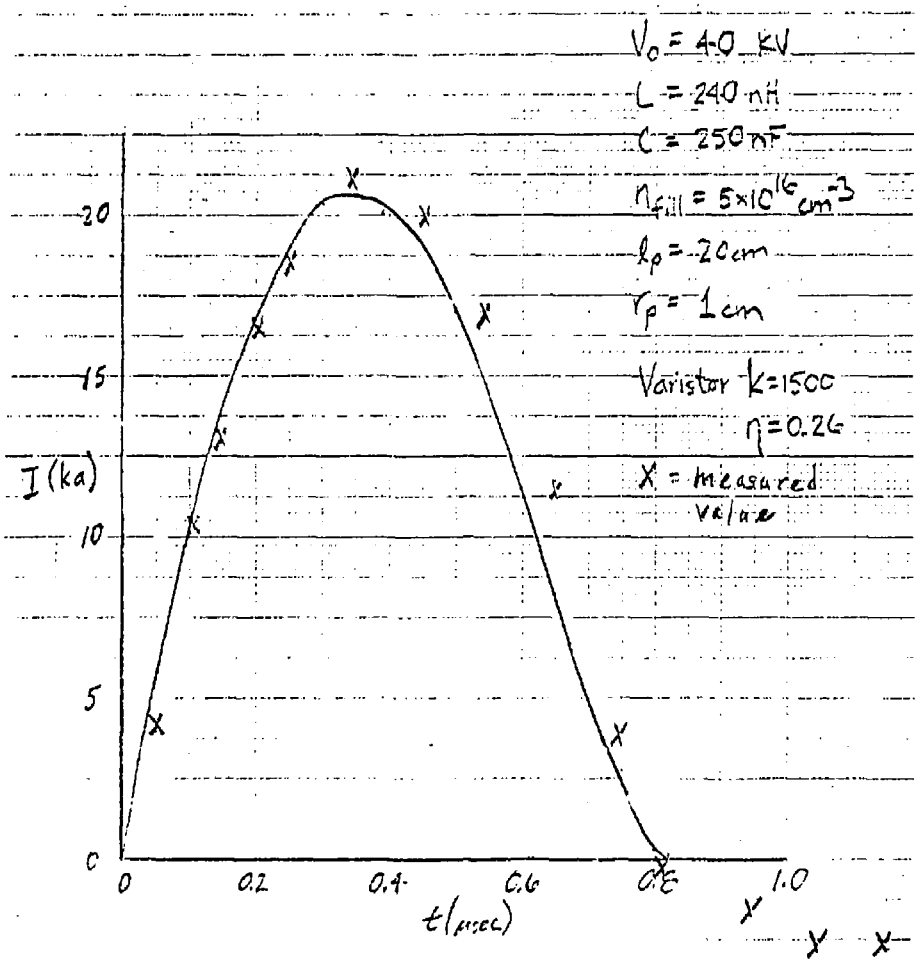

Figure 1. Comparison of Calculated and Measured Preionization Waveform with Varistor Damping

device and allowed simultaneous operation of both devices at their maximum charging voltages of 20 kV and 40 kV, respectively. A confining field, B_z, of 35 kGauss could thus be obtained in the sample volume.

3. Changes to Experimental Arrangement for Improved Optical Access

In order to accommodate the streak spectrometer for simultaneous observation of the plasma sample, changes to the experimental arrangement indicated on Figure 3 were made. The Korad ruby laser was removed to a remote table, actually the CO_2 laser diagnostic table, and the corner turning mirror "A" was removed from the optical support bridge and supported on a rigid cantilever arm over the laser. In the area vacated by moving the ruby laser, a new optical support table was constructed to support the streak spectrometer, which ten viewed the plasma sample at the port marked "optional access" on Figure 3.

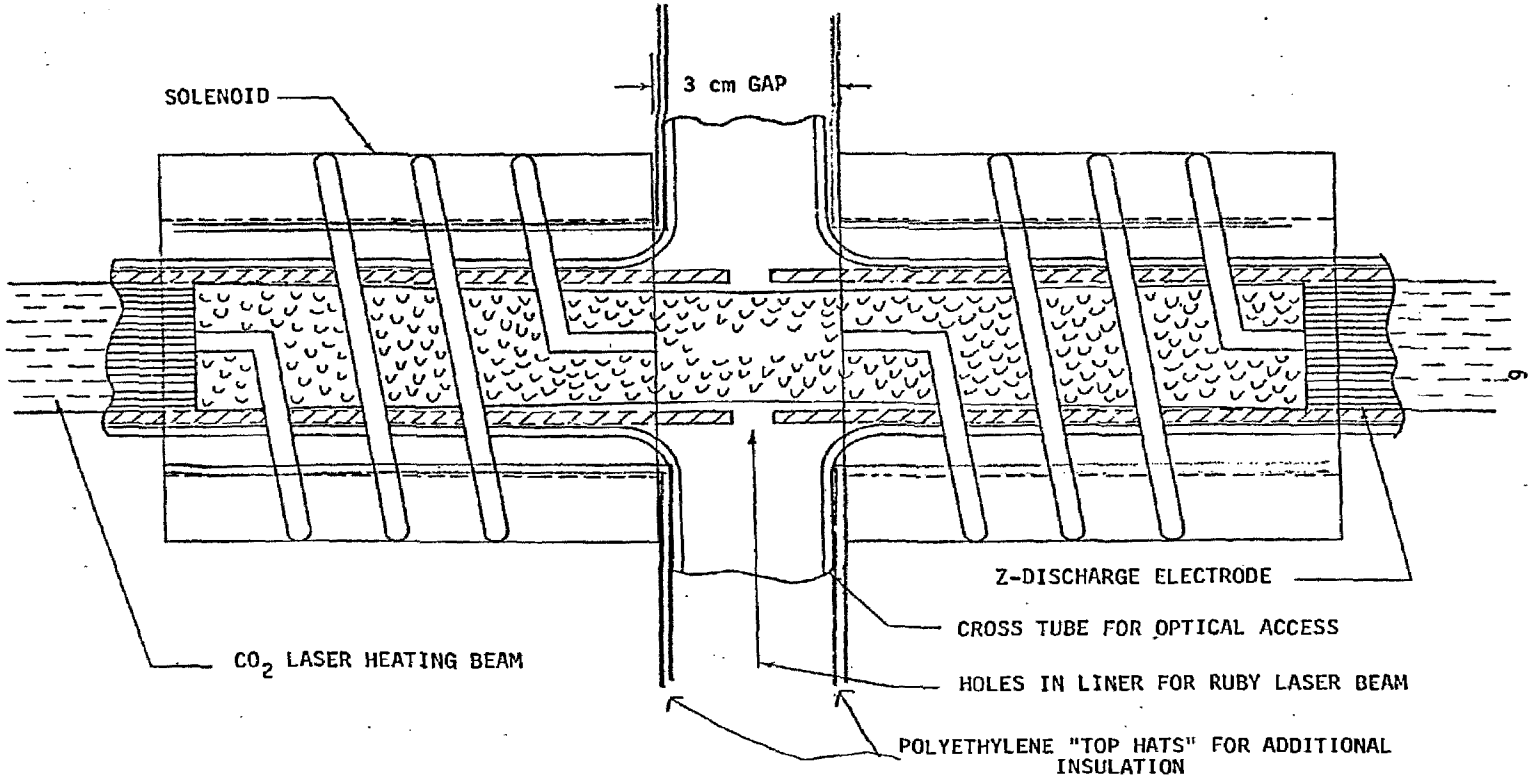

Figure 2. Solenoid Assembly, Showing Glass Cross, Tube Liner, and Z-Discharge Electrodes in Place

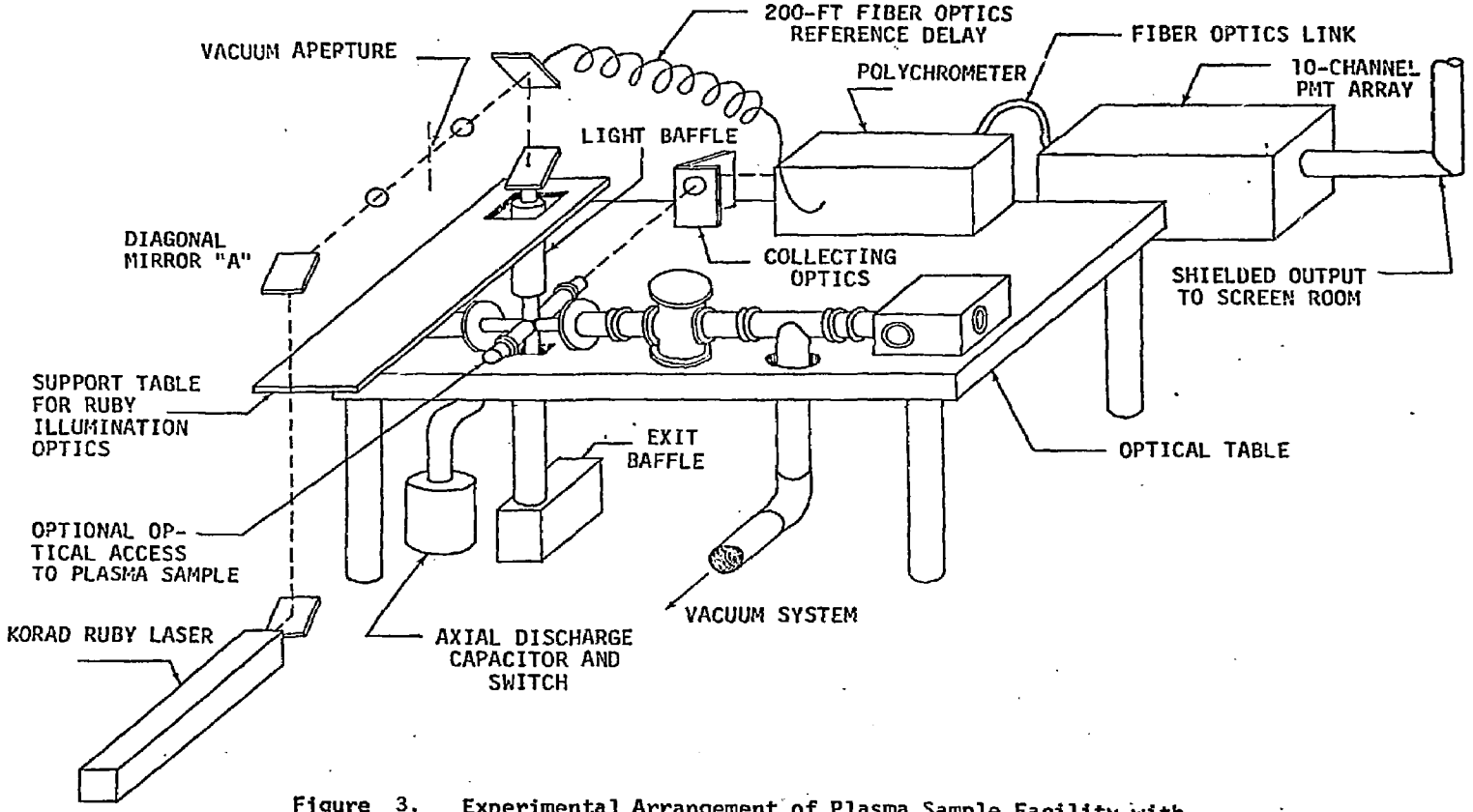

Figure 3. Experimental Arrangement of Plasma Sample Facility with Thomson Scattering Diagnostic in Place

76 00595

SECTION III

EXPERIMENTAL RESULTS

The experimental methodology used in this work was the same in all respects as that reported in Reference 1, except for the addition of the streak spectrometer, and the modified preionization discharge. The solenoid was operated at V_0 = 10 kV, producing a field of 17 kGauss. The chamber was filled to a pressure of approximately 0.75 torr of sample gas, giving $n_{fill} = 5 \times 10^{16}$. The preionization discharge was started 5.5 μsec after the start of the solenoid, and the heating laser fired approximately 2.0 μsec later--that is nearly at peak B_Z. The streak spectrometer was started at the same time as the preionization discharge, or in some cases 1.0 μsec later, and operated with a 5 μsec streak duration.

The probe laser for the Thomson scattering diagnostic was operated at various times after the heating laser pulse, and the times recorded. As an additonal check of the probe laser timing, the ruby laser pulse can be seen on most of the hard film streak spectra as a small dot approximately 2.5 mm to the red side of the D_α line. The small spectral width of the dot indicates that it is either the Thomson scattering ion feature, stray light at λ_0, or a combination of both. Additional intensification of the image would be necessary to observe the electron feature. The laser start time seems to also be indicated clearly on the streak spectra by an abrupt dimming of the higher order D lines.

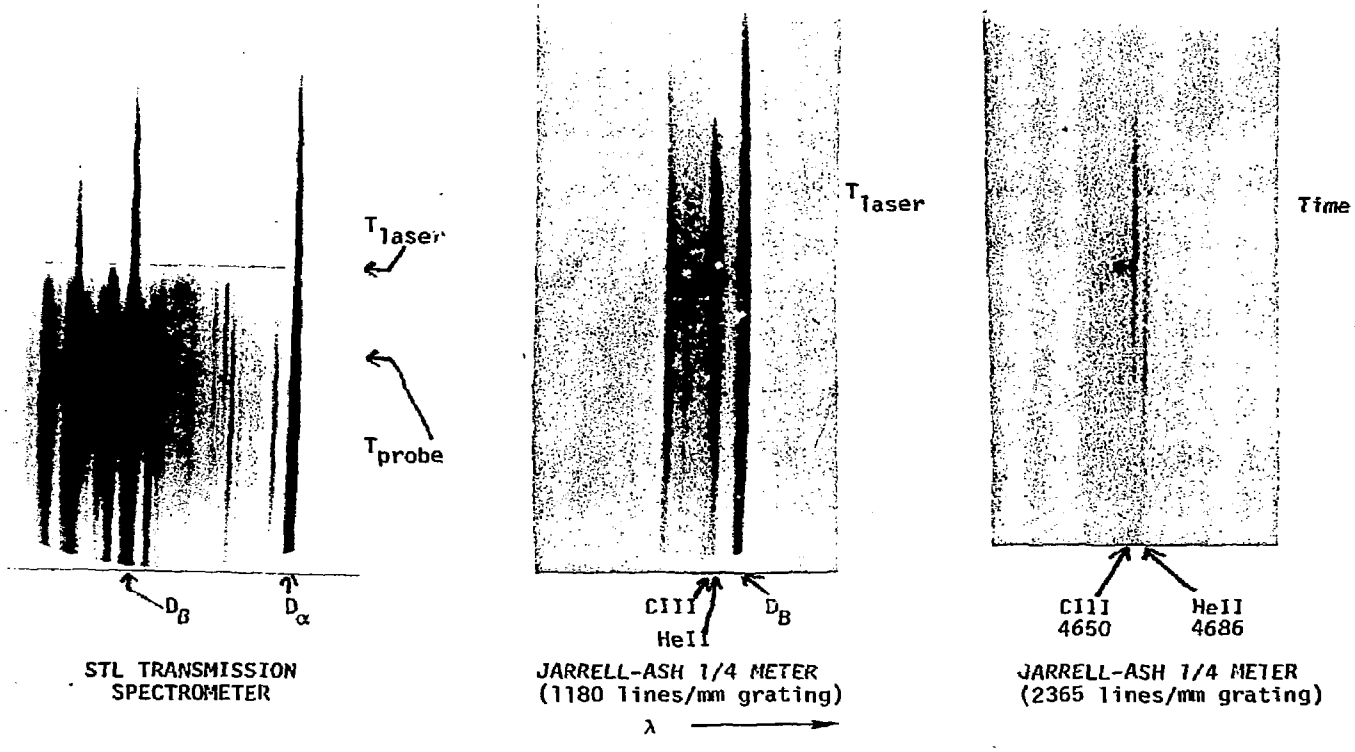

Figure 4. Typical Streak Spectra with Various Spectrometer Configurations, D_2 + 3% C + 5% He Plasma. Streak Speed 0.43 μsec/cm at this scale

The streak spectrometer consisted of an STL model 2D streak camera with a Varian single stage intensifier attached to the relay camera. A spectrometer was focused on the photocathode of the STL camera, and was one of two types. An STL model 42D transmission spectrograph was used for most experiments and gave coverage of the full visible spectrum, but the resolution of the camera system was inadequate for some purposes with this device. In order to clearly separate the HeII line at 4686 A and the CIII line at 4650 A, a Jarrell-Ash 1/4 meter monochrometer was set up and focused on the streak camera. It was tried with both 1180 L/mm and 2365 L/mm gratings while set at $\lambda_6 \approx 4600$ Å. Typical results may be seen in Figure 4 with various features identified. Note that very adequate separation of the HeII and CIII lines is obtained with the 2340 L/mm grating, but its 3000 Å blaze makes its use inefficient in this spectral range. Most of the film spectra obtained were sent to LLL for calibration, development and interpretation (40 films in all), AA1 through A5-4, and analysis is not yet complete.

The accompanying Thomson scattering spectra were analyzed according to the procedures discussed in Reference 1. The resulting computer fitted curves are shown in Figures 5 through 19 along with the values of the scattering parameter α and the values of the plasma parameters n_e and T_e inferred from the best fit spectrum. The figure caption indicates the plasma sample conditions and probe time along with specific film identification numbers when applicable. Figure 20 summarizes the result of heating experiments using 150 joules of laser energy plotted on the same scale as Figure 3.13 of Reference 1 with

the new points differentiated using new symbols (3rd series and 4th series). Note reasonable reproducibility of the results for the plasma temperature. The plasma density has been increased to very nearly n_0, probably due to the use of the new preionization system. The lower density could easily be reached by lowering the fill pressure.

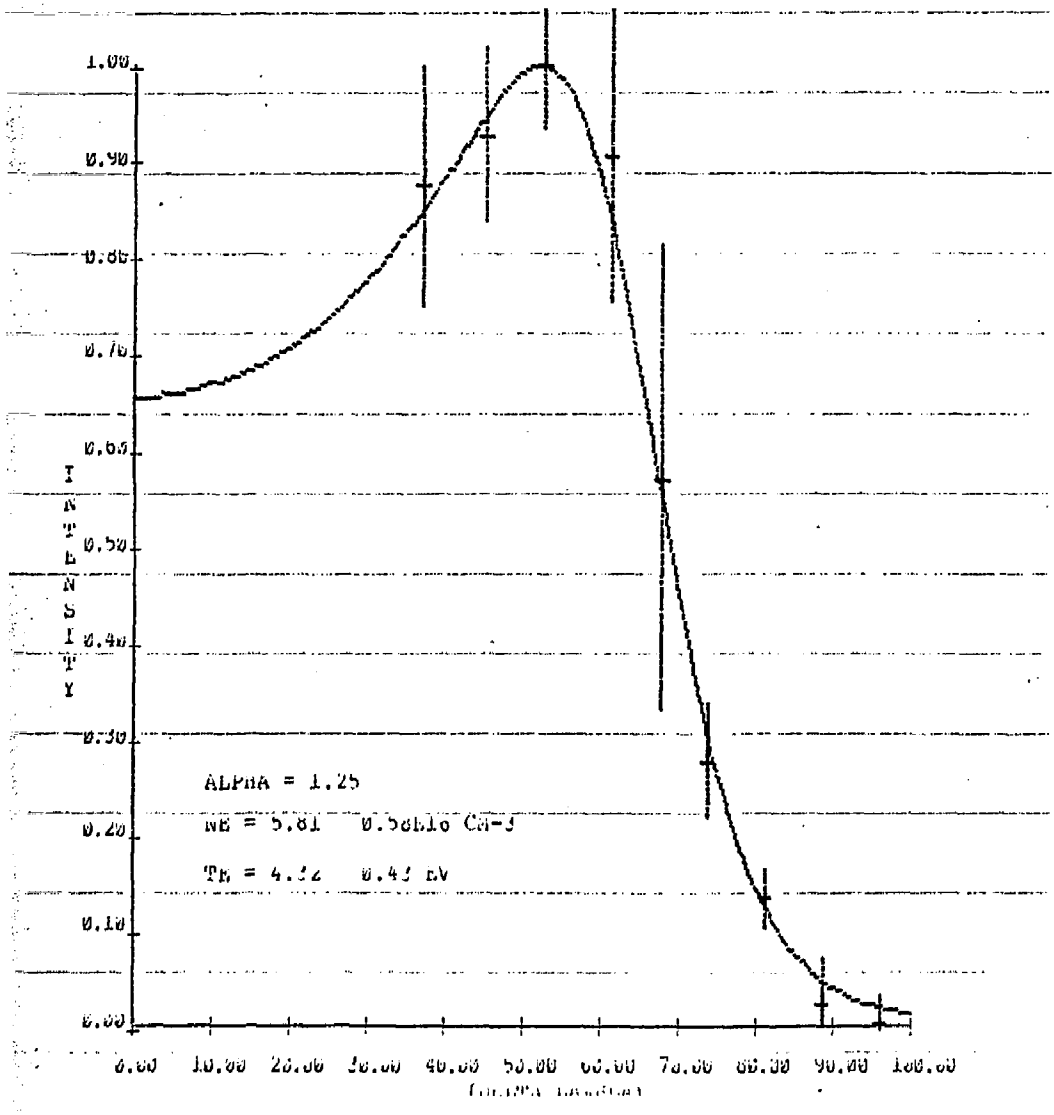

Figure 5. Thomson Scattering Spectrum Result, D_2 + 3% C + 5% He Plasma $n_{fill} = 5 \times 10^{16}$ Heated with 150 Joules of Laser Energy, B_z = 17 kGauss, Probe Time 1.4 usec after Laser Heating. This is an ensemble of 5 events including those correlated with film numbers AA1, #1.

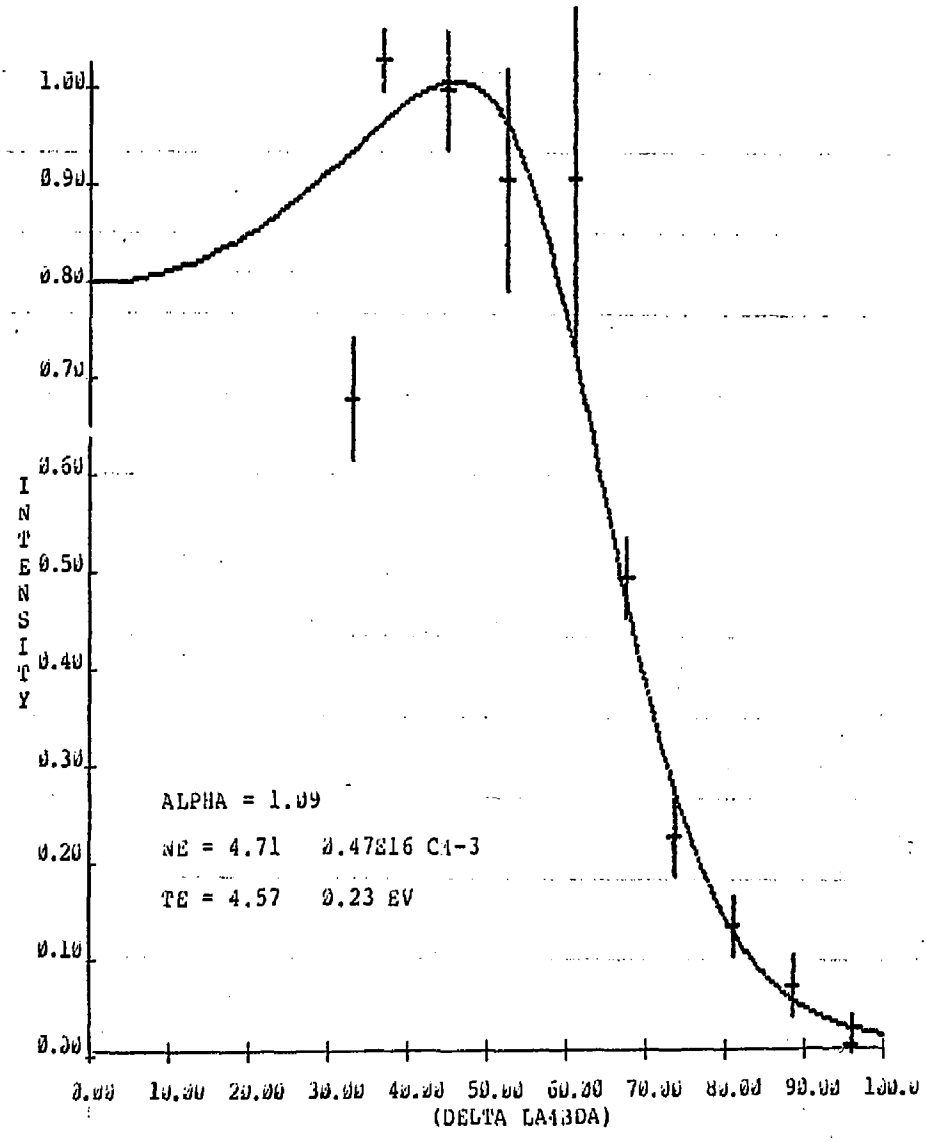

Figure 6. Thomson Scattering Spectrum Result, D_2 + 3% C + 5% He Plasma $n_{fill} = 5 \times 10^{16}$ Heated with 150 Joules of Laser Energy, B_z = 17 kGauss, Probe Time 1.0 μsec after Laser Heating. This is an ensemble of 2 events including those correlated with film numbers #4, AB1.

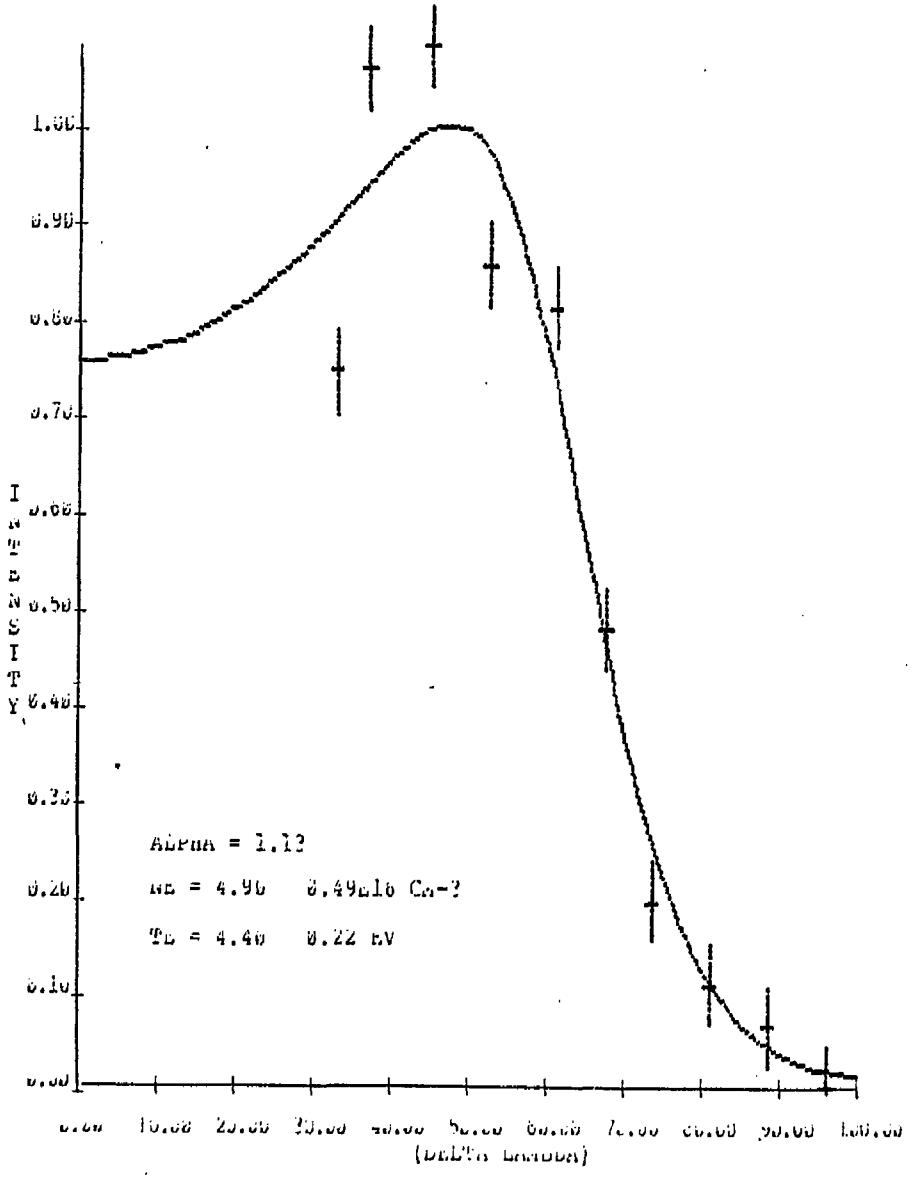

Figure 7. Thomson Scattering Spectrum Result, D_2 only Plasma $n_{fill} = 5 \times 10^{16}$ Heated with 150 Joules of Laser Energy, B_z = 17 kGauss, Probe Time 1.0 μsec after Laser Heating. This is an ensemble of 1 event.

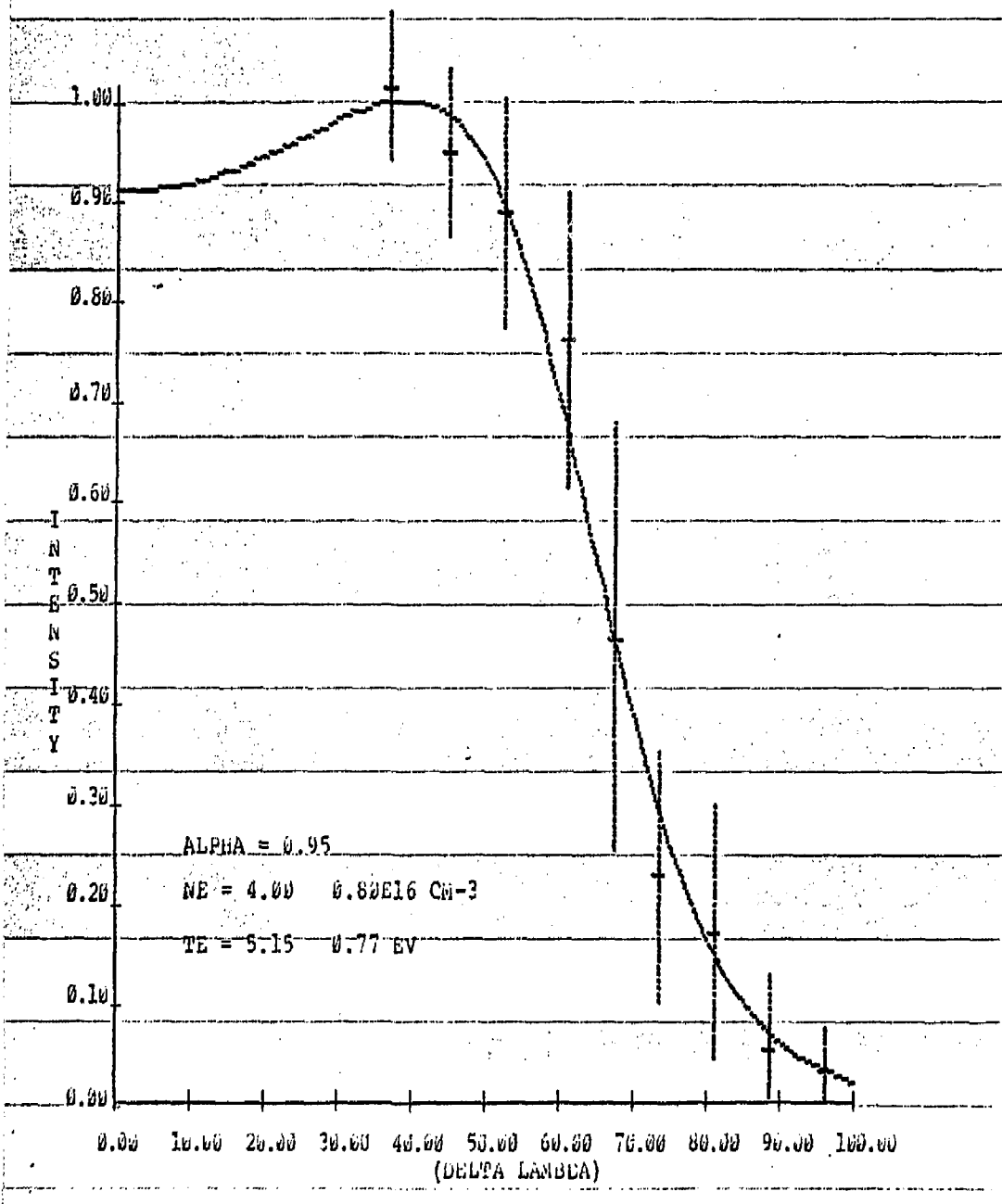

Figure 8. Thomson Scattering Spectrum Result, D_2 only Plasma $n_{fill} = 5 \times 10^{16}$ Heated with 150 Joules of Laser Energy, $B_z = 17$ kGauss, Probe Time 1.0 μsec after Laser Heating. This is an ensemble of 5 events including those correlated with film numbers AC-3, #5.

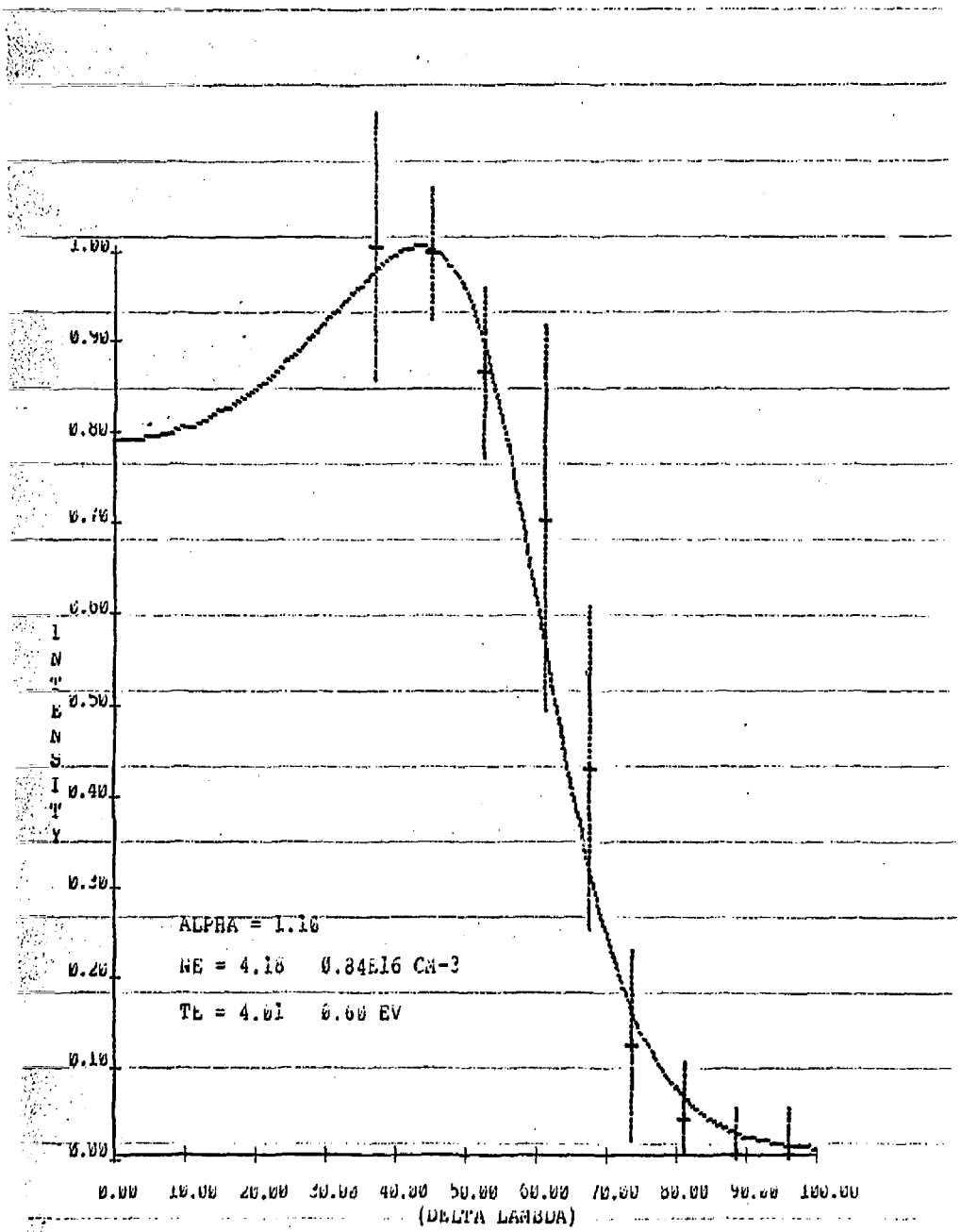

Figure 9. Thomson Scattering Spectrum Result, D_2 + 3% C + 5 He Plasma $n_{fill} = 5 \times 10^{16}$ Heated with 150 Joules of Laser Energy, B_z = 17 kGauss, Probe Time 0.8 μsec after Laser Heating. This is an ensemble of 5 events including those correlated with film numbers AD-1, AD-2, AD3, #6.

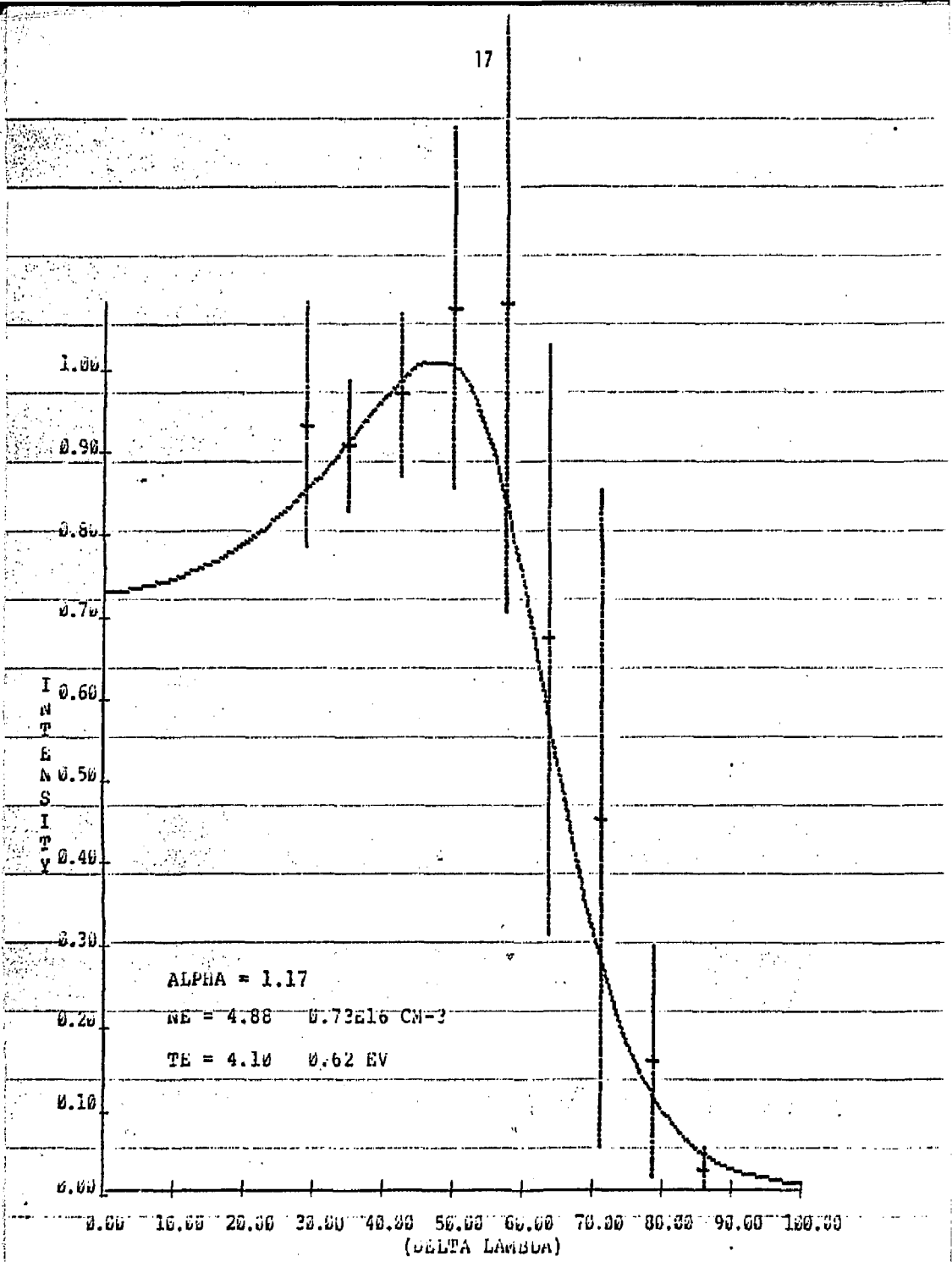

Figure 10. Thomson Scattering Spectrum Result, D_2 + 3% C + 5% He Plasma $n_{fill} = 5 \times 10^{16}$ Heated with 115 Joules of Laser Energy, B_z = kGauss, Probe Time 0.8 μsec after Laser Heating. This is an ensemble of 4 events.

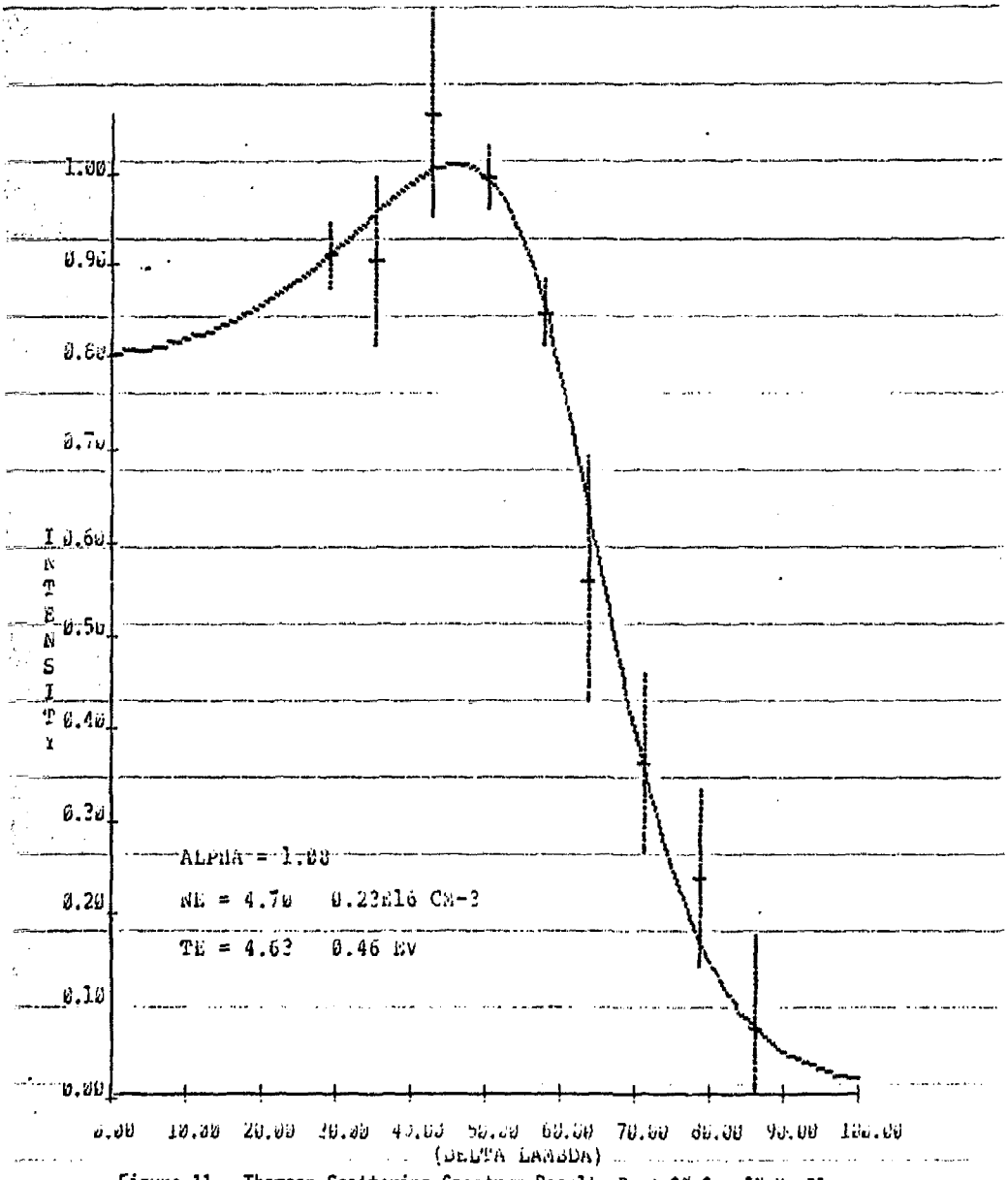

Figure 11. Thomson Scattering Spectrum Result, D_2 + 3% C + 5% He Plasma $n_{fill} = 5 \times 10^{16}$ Heated with 170 Joules of Laser Energy, B_z = 17 kGauss, Probe Time 0.8 μsec after Laser Heating. This is an ensemble of 2 events including those correlated with film number #7.

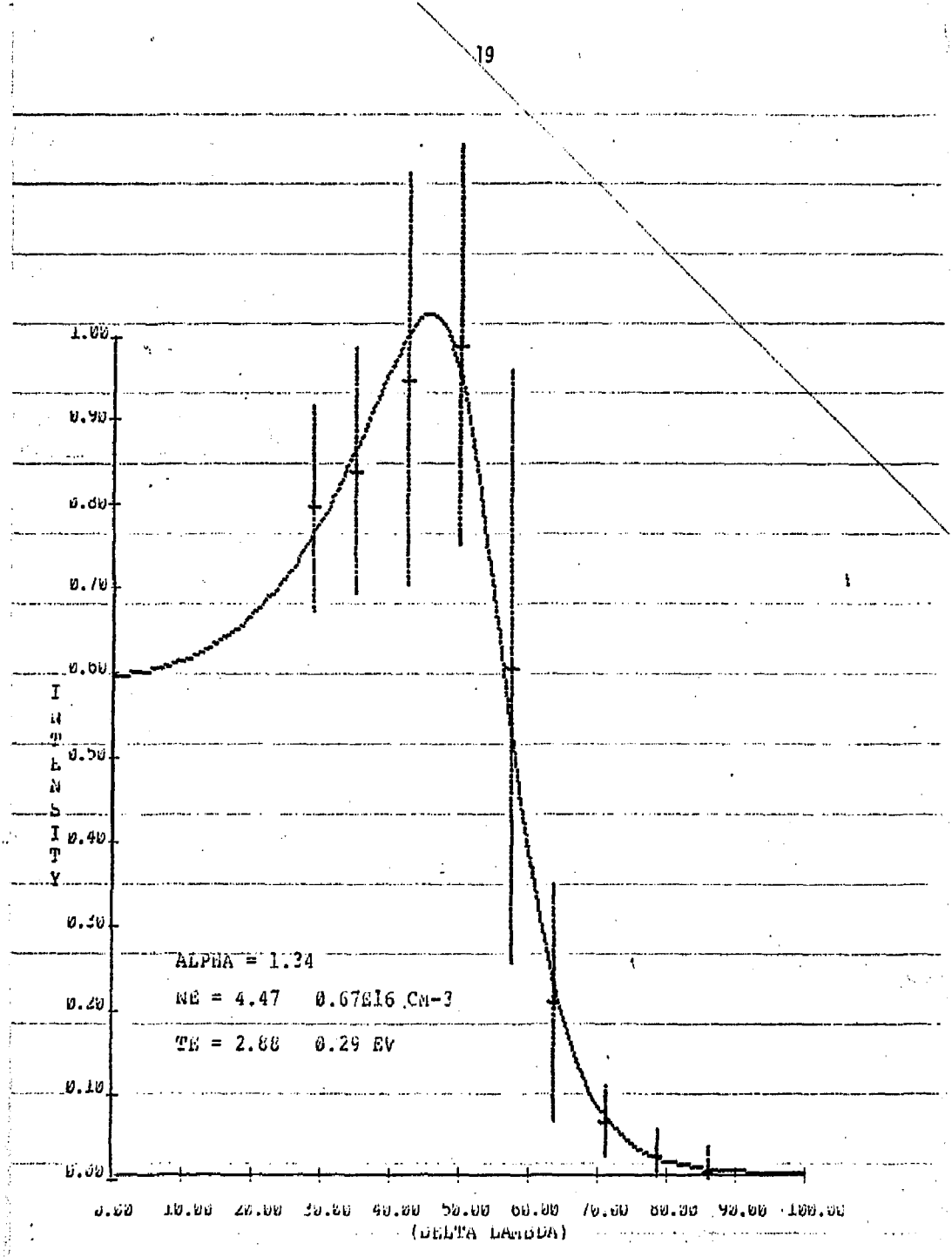

Figure 12. Thomson Scattering Spectrum Result, D_2 + 3% C + 5% He Plasma $n_{fill} = 5 \times 10^{16}$ Heated with 100 Joules of Laser Energy, B_z = 17 k Gauss, Probe Time 2.2 μsec after Laser Heating. This is an ensemble of 5 events including those correlated with film numbers AE-3, AF-2.

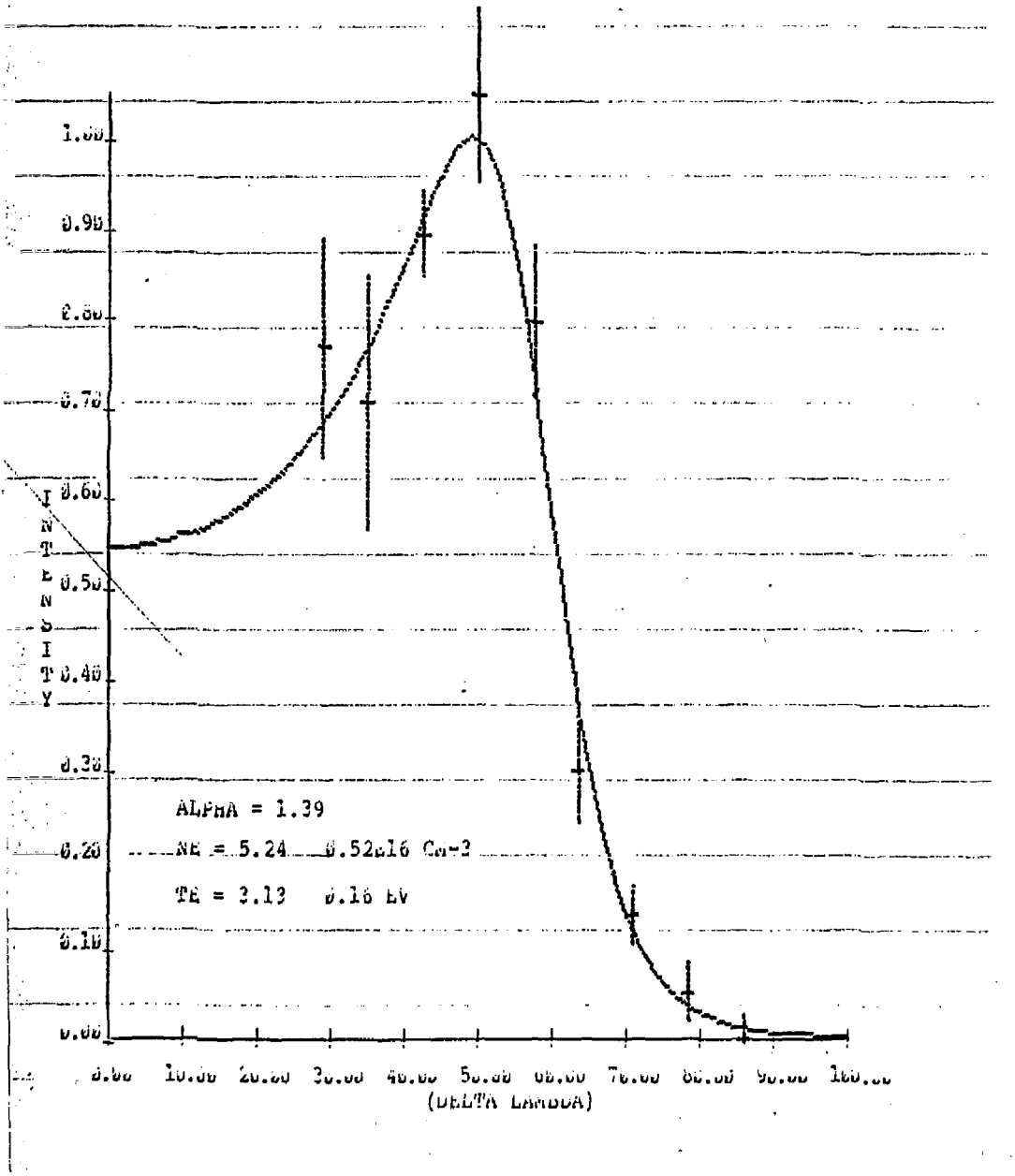

Figure 13. Thomson Scattering Spectrum Result, D_2 + 3% C + 5% He Plasma $n_{fill} = 5 \times 10^{16}$ Heated with 123 Joules of Laser Energy, B_z = 17 kGauss, Probe Time 2.2 μsec after Laser Heating. This is an ensemble of 5 events including those correleated with film number AE-1.

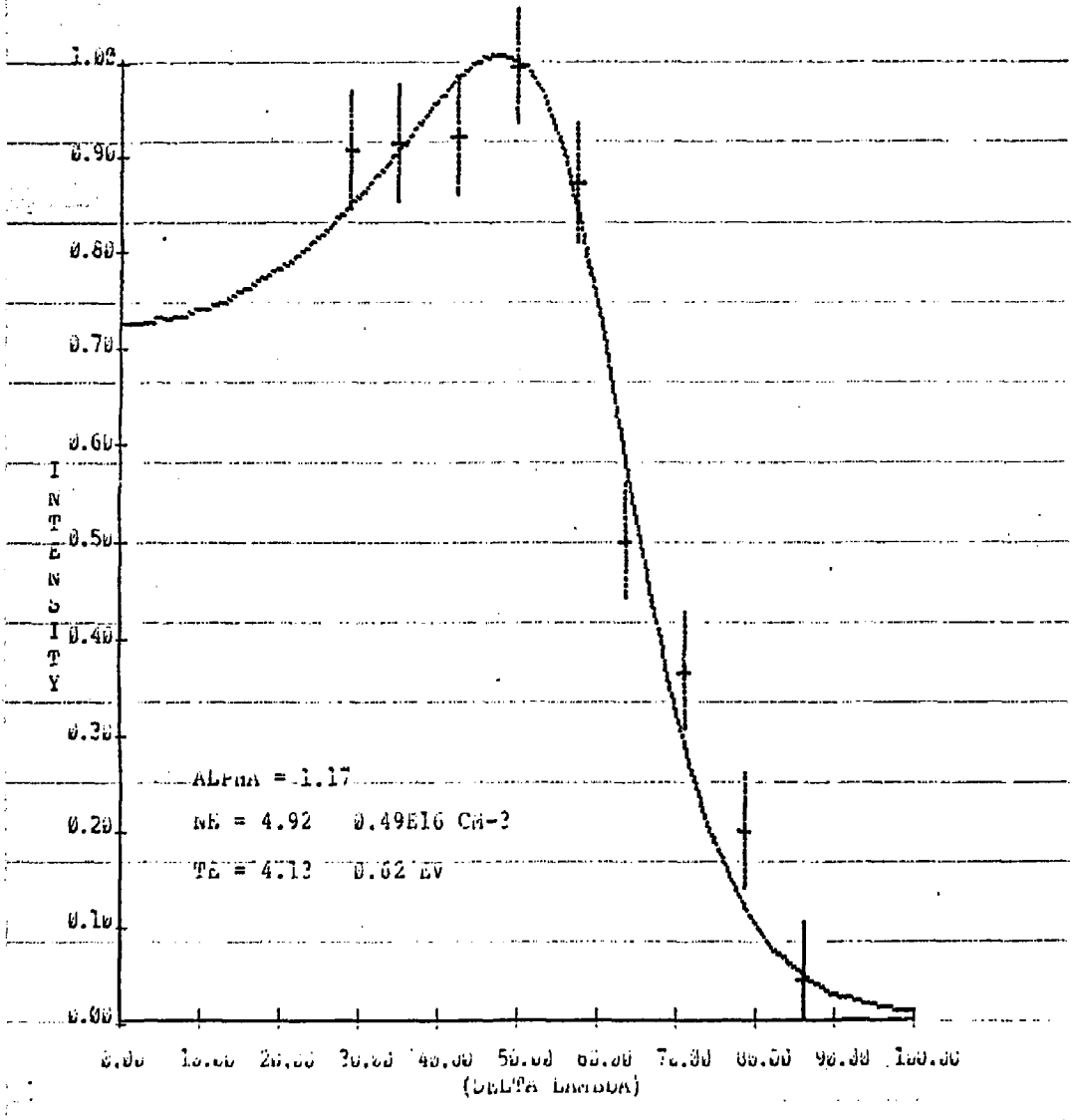

Figure 14. Thomson Scattering Spectrum Result, D_2 + 3% C + 5% He Plasma n_{fill} = 5 x 10^{16} Heated with 153 Joules of Laser Energy, B_z = 17 kGauss, Probe Time 2.2 μsec after Laser Heating. This is an ensemble of 1 event.

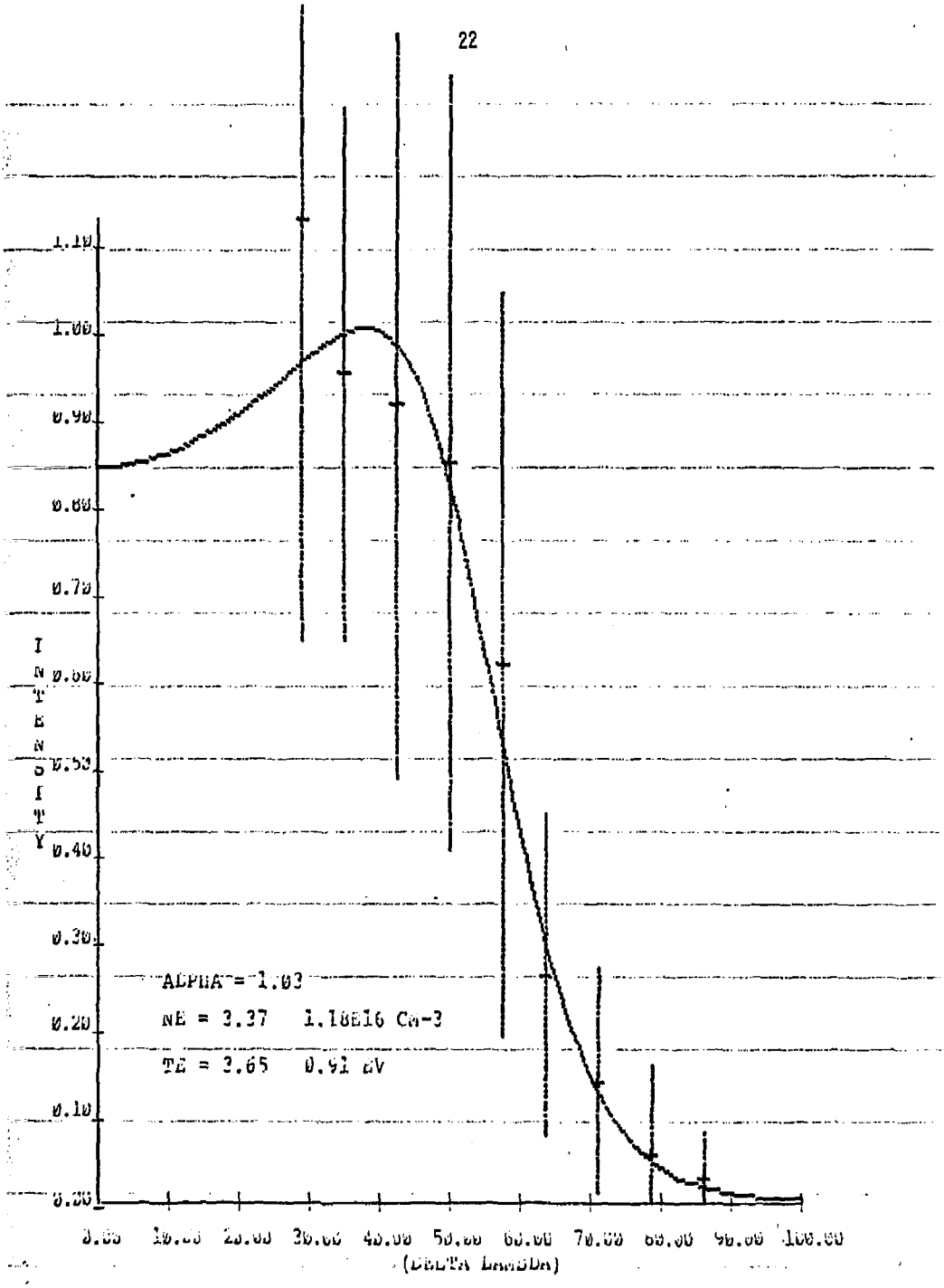

Figure 15. Thomson Scattering Spectrum Result, D_2 + 3% C + 5% He Plasma $n_{fill} = 5 \times 10^{16}$ Heated with 100 Joules of Laser Energy, B_z = 17 k Gauss, Probe Time 1.7 μsec after Laser Heating. This is an ensemble of 4 events including those correlated with film number AF-3.

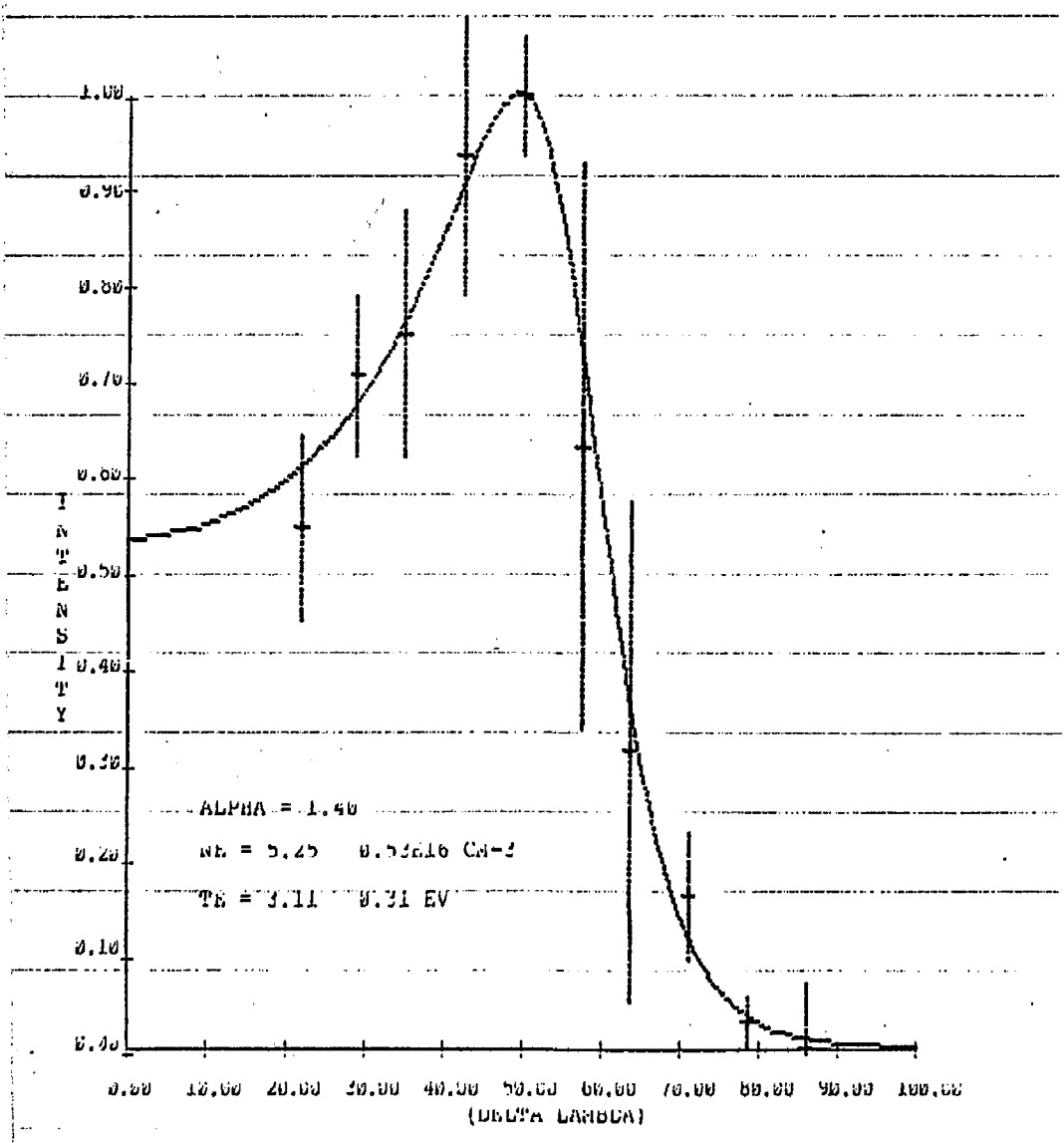

Figure 16. Thomson Scattering Spectrum Result, D_2 + 3% C + 5% He Plasma n_{fill} = 5 x 10^{16} Heated with 80 Joules of Laser Energy, B_Z = 17 kGauss, Probe Time 1.5 μsec after Laser Heating. This is an ensemble of 3 events including those correlated with film numbers AG-2, AG-3.

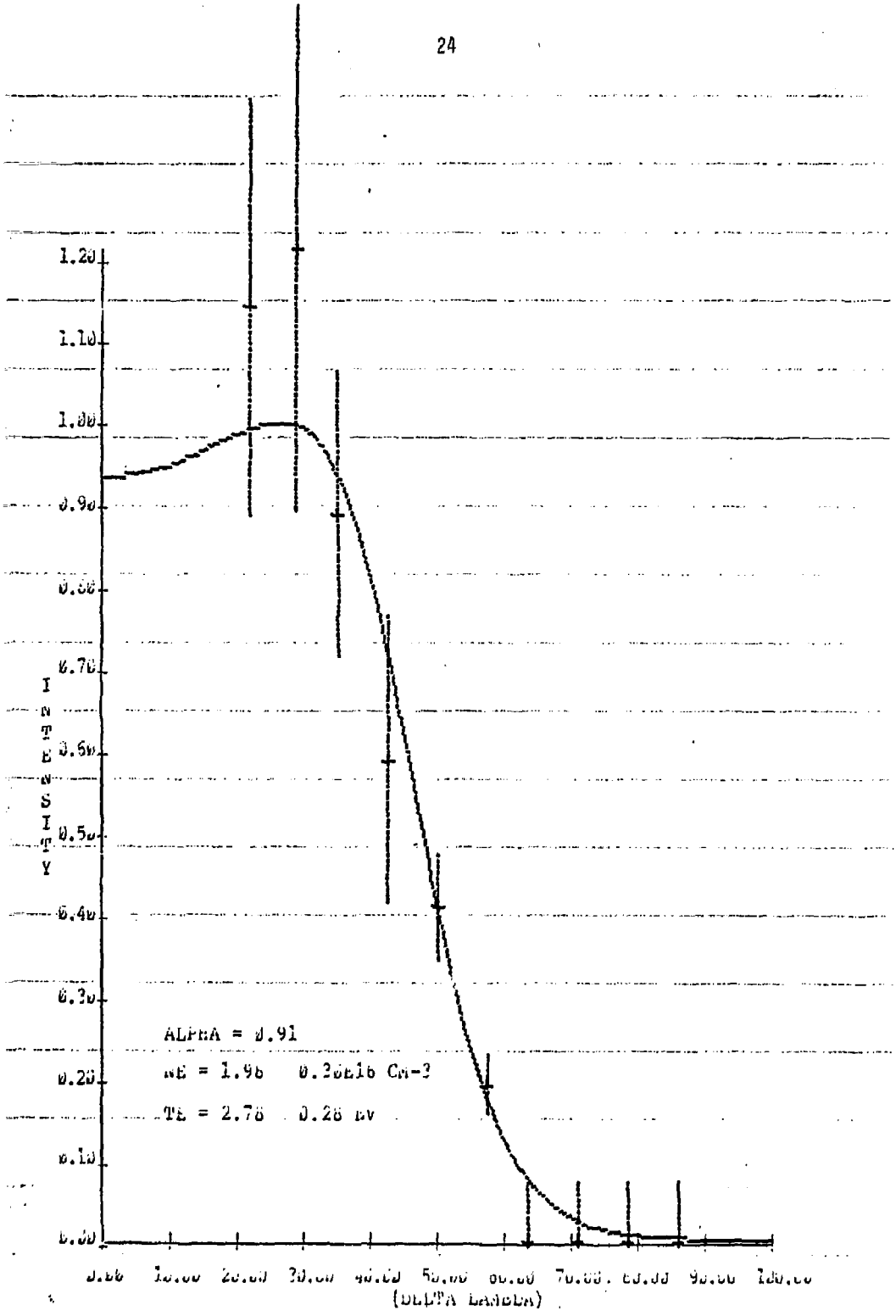

Figure 17. Thomson Scattering Spectrum Result, D_2 + 3% C + 5% He Plasma $n_{fill} = 5 \times 10^{16}$ Heated with 80 Joules of Laser Energy, B_z = 17 kGauss, Probe Time 1.4 μsec after Laser Heating. This is an ensemble of 3 events including those correlated with film number AH-2.

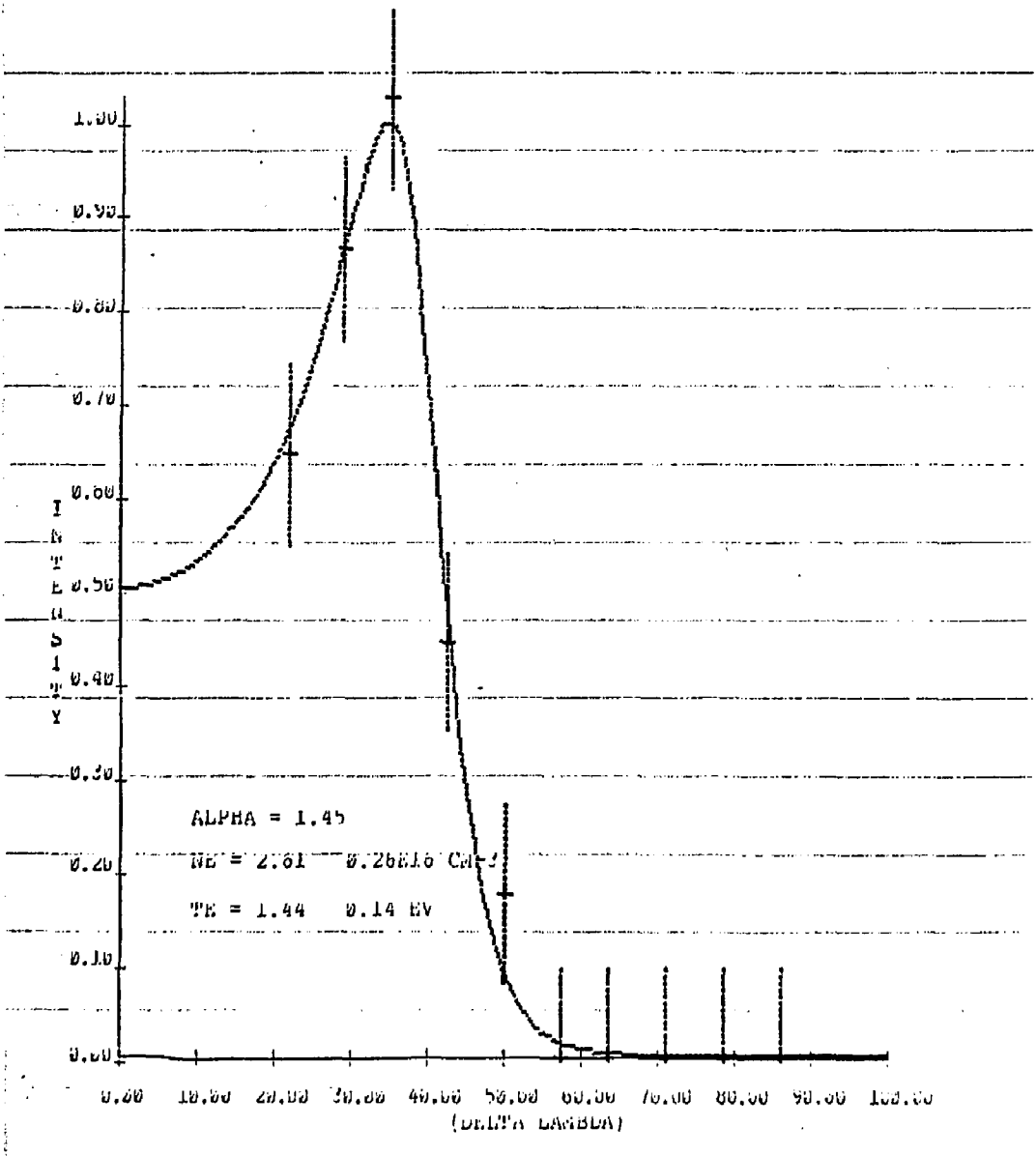

Figure 18. Thomson Scattering Spectrum Result, D_2 + 3% C + 5% He Plasma $n_{fill} = 5 \times 10^{16}$ Heated with 38 Joules of Laser Energy, B_z = 17 kGauss, Probe Time 1.5 μsec after Laser Heating. This is an ensemble of 1 event including those correlated with film number AH-1.

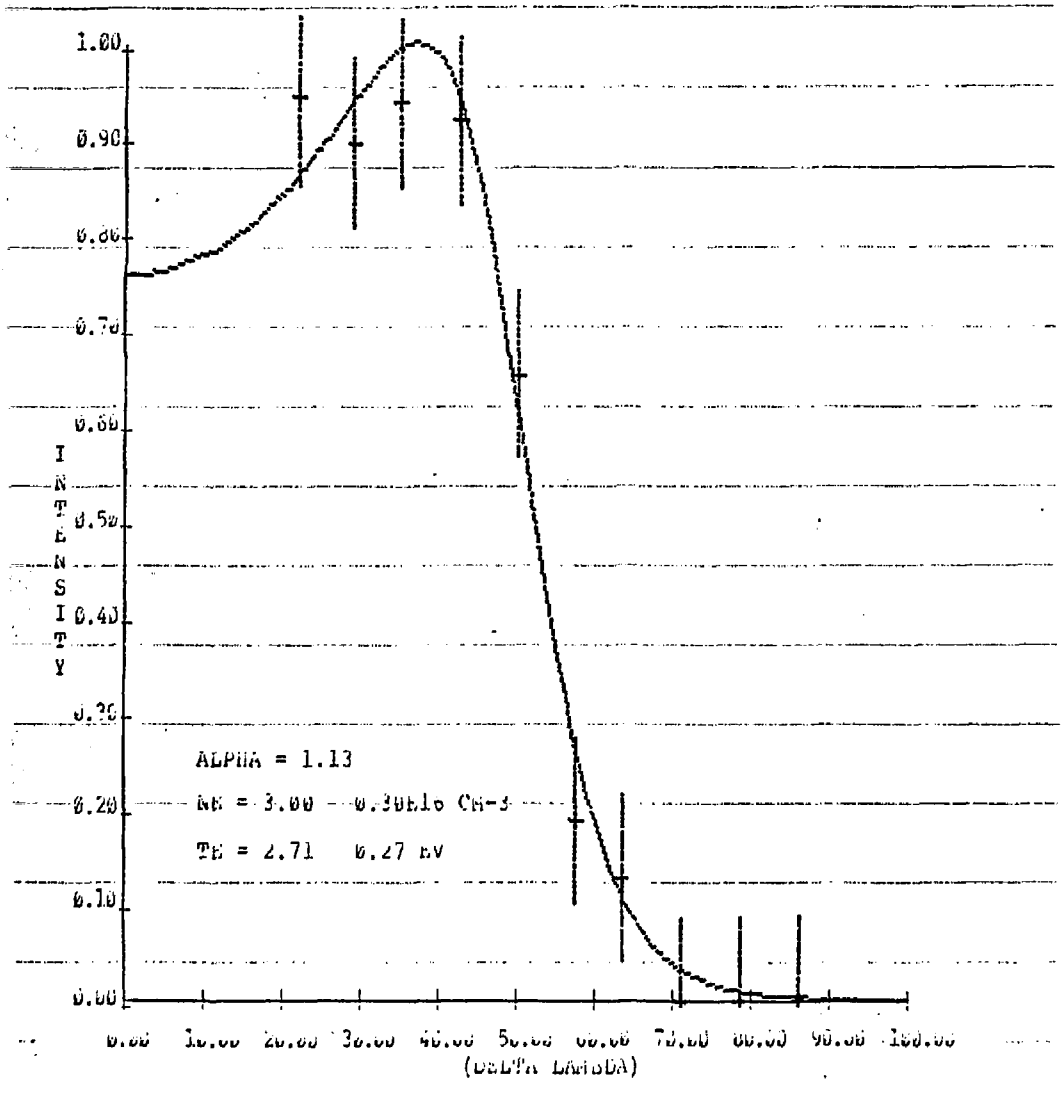

Figure 19. Thomson Scattering Spectrum Result, D_2 + 3% C + 5% He Plasma $n_{fill} = 5 \times 10^{16}$ Heated with 85 Joules of Laser Energy, B_z = 17 kGauss, Probe Time 1.5 μsec after Laser Heating. This is an ensemble of 1 event including those correlated with film number AG-1.

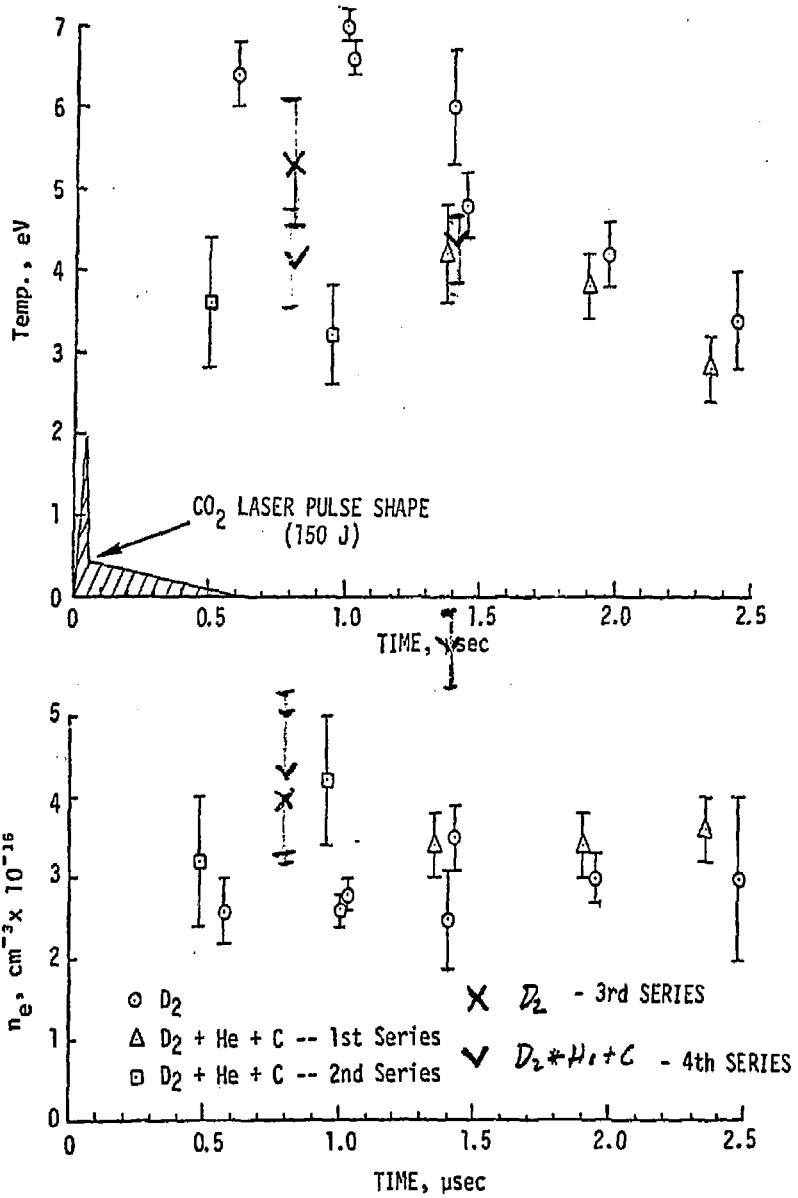

Figure 20. Plasma Parameters (Cooling Curves) as Determined by Ensemble Averaged Thomson Scattering Spectra. Deuterium Filling at $n_o = 5 \times 10^{16}$ cm^{-3}, ⊙; Deuterium + 5 % Helium + 3 wt% Carbon Shown by △; ⊡. All Cases Heated with 150-J 10.6 μ Radiation, 2 μsec after Peak of Preionization Discharge. 1st and 2nd Series, 1976 data; 3rd and 4th Series, 1977 data.

SECTION IV

THEORETICAL SUPPORT

The effects of modifying the preionization circuit with varistor damping have been estimated using a simple homogeneous Ohmic-heating model. Radial heat losses by heat conduction and charge exchange with neutral particles have also been estimated. These calculations are described in detail below. In addition, axial laser heating calculations for the present experimental conditons, with and without carbon line radiation losses, have been completed and are presently being analyzed.

4.1. Preionization Discharge

A simple zero-dimensional model of an axial preionization discharge in hydrogen gas was developed under the previous LLL contract. This section reports recent calculations using this model with revised energy losses and varistor circuit damping. It is shown that the use of a single high current pulse with minimal backswing may make a significant change in the preionization conditions, increasing the average electron density by 35 percent.

Energy losses. The details of the three-fluid model have been described in a previous report.[1] The model describes the energy balance for Ohmic heating and ionization of a homogeneous hydrogen plasma containing

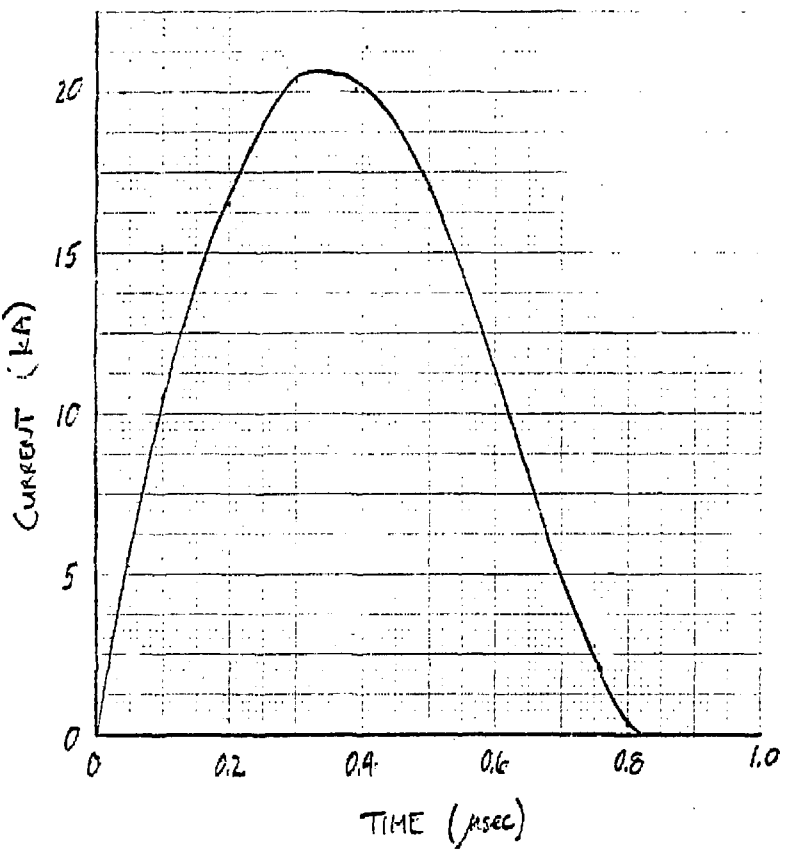

Figure 21. Calculated Z-Discharge Current Waveform for Typical Circuit Parameters (V_o = 40 kV, L = 240 nH, C = 250 nf, $n_{fill} = 5^{o} \times 10^{16}$ cm^{-3}, ℓ_p = 20 cm, r_o = 1 cm, and varistor k = 1500 and η = 0.26)^{p}

neutrals, ions, and electrons. The energy source is axial currents provided by an external circuit. It was found that this model overestimated the degree of ionization reached for most circuit conditions and filling pressures. The model was compared with electron density measurements made by interferometry and Thomson scattering. To obtain agreement between the theory and experiment, it has been necessary to use an effective ionization energy of 50 eV to account for hydrogen dissociation energy, energy lost to the wall, and radiation losses. Such a value has been suggested by other investigators in this field.[2] By using an effective ionization energy, the total energy losses per unit volume are calculated to be

$$E_L = \int_0^t n n_0 S[\chi_{eff} - \chi_H] \, dt'$$

where χ_{eff} is the effective ionization energy (50 eV), χ_H is the actual ionization energy (13.6 eV), S is the ionization coefficient, n is the electron density, and n_0 is the neutral density.

Varistor Circuit. The axial current is determined by an external circuit. The experiment has been modified to include varistor damping to produce a single high-current pulse. The varistor damping resistance is approximated by the formula given by DeSilva and Pechacek[3]

$$R_D = k|I|^{n-1}$$

For the varistor used here, the values are k = 1500 and n = 0.26. The predicted current waveform for typical circuit conditions is given in Figure 21. The peak current is approximately 45 percent higher than with critical damping.

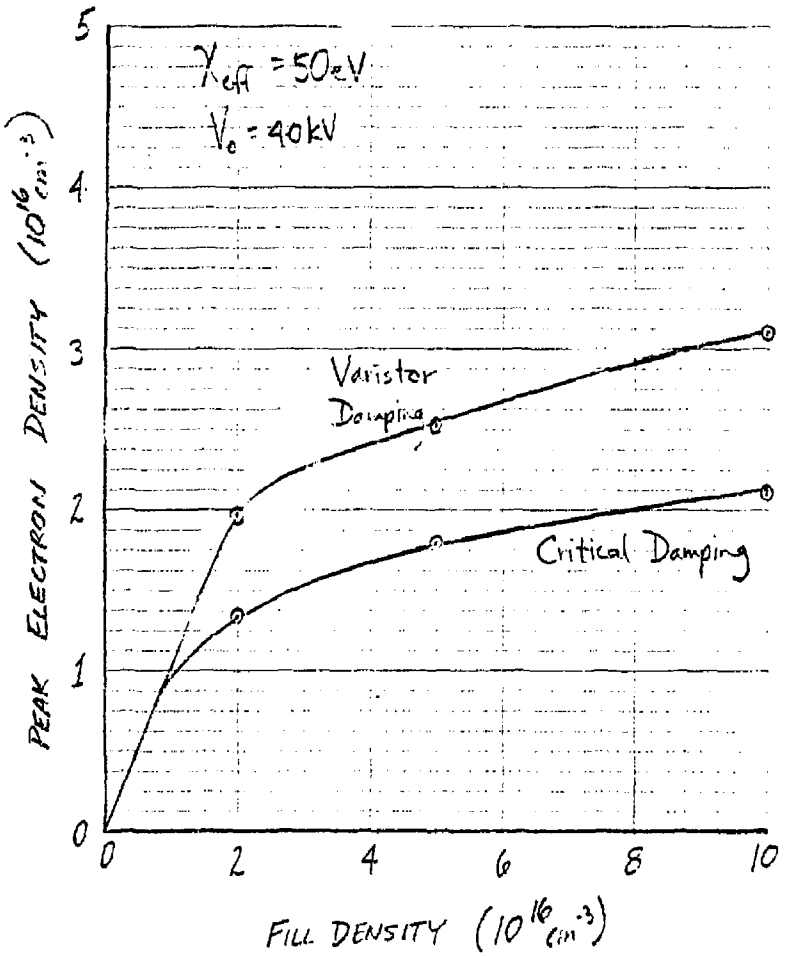

Figure 22. Predicted Preionization Density as a Function of Initial Filling Density for Critically Damped and Varistor Damped Circuits; Charging Voltage 40 kV; 50-eV Effective Ionization Energy

Results. The calculated peak electron density reached using critically damped and varistor damped circuits is compared in Figure 22. This simple model predicts that the use of varistor damping will increase the preionization level by about 35 percent for a filling density of 5×10^{16} cm^{-3}. Measurements of the actual centerline electron density following varistor-damped preionization have not been made at this time. However, the observed increase in *centerline electron density after laser heating indicates that changing* the preionization current pulse has a strong effect on reducing neutral particle losses. The magnitude of energy losses estimated by using a 50 eV effective ionization energy may be seen in Figure 23 which shows the time dependence of particle and energy densities for $n_{fill} = 5 \times 10^{16} cm^{-3}$.

4.2. Energy Balance

Previous experiments in the LLL sponsored plasma sample test facility have indicated the presence of unexpectedly rapid cooling rates.[1] Light scattering measurements of a deuterium plasma at the column centerline showed T_e decaying from approximately 7 eV to 3.5 eV in the 2-μsec observation time. The plasma density remains constant, within experimental error, at $n_e \sim 3 \times 10^{16} cm^{-3}$.

The observed cooling rate is not well understood. The only effect considered in previous studies which comes close to being able to account for the losses is classical radial heat conduction. In an

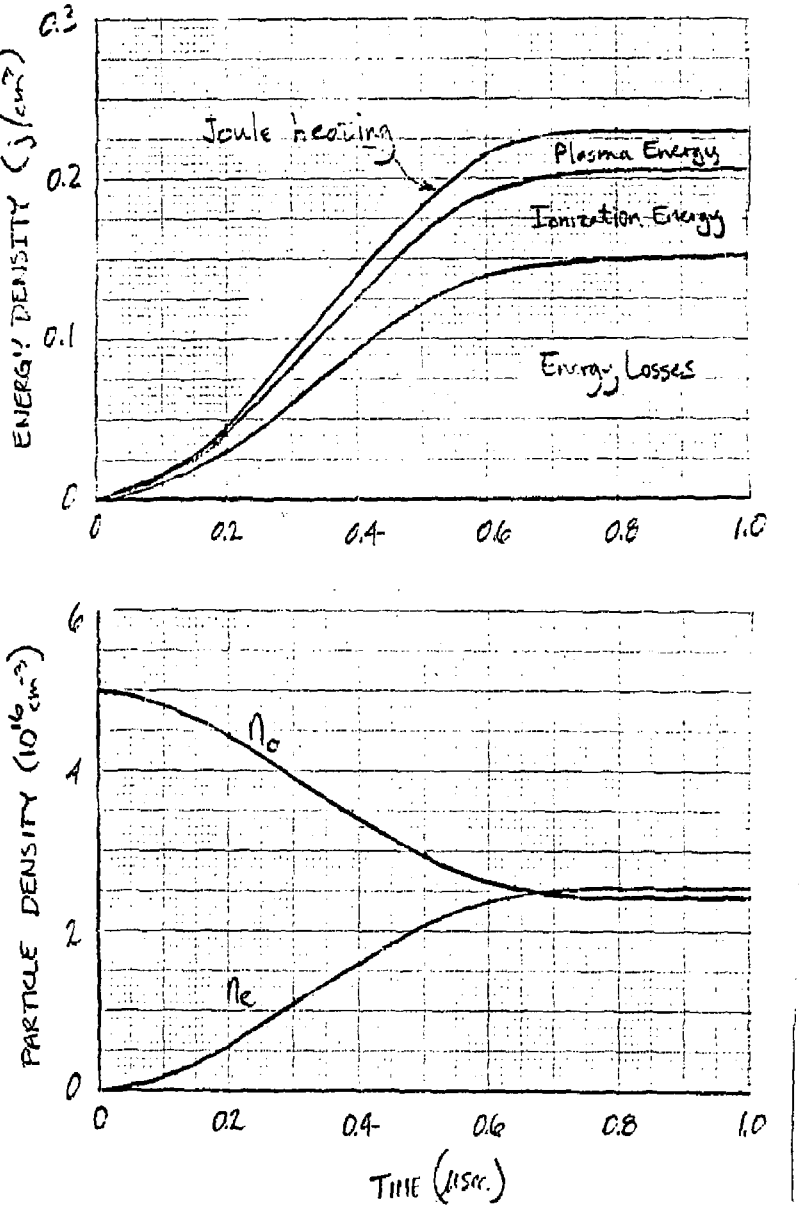

Figure 23. Time Dependence of Particle and Energy Densities in Homogeneous Z-Discharge; Fill Density 5×10^{16} cm^{-3}; Charging Voltage 40 kV; Energy Losses Approximated by 50-eV Effective Ionization Energy

attempt to reduce radial heat losses, the experiment has been upgraded to increase the axial magnetic field in the observation region from 1.7 Tesla to 3.5 Tesla. This section reports recent calculations of radial heat flow which take into account the temperature dependence of thermal conductivity.

Another effect which has been postulated to possibly account for the observed losses is charge exchange with cold neutrals. A cold boundary layer is apparently formed near the tube wall during the diffusive axial preionization discharge prior to laser heating as evidenced by the observed electron density ($n_e \sim 3 \times 10^{16} cm^{-3}$ for a filling density of $n_0 = 5 \times 10^{16} cm^{-3}$). The effect of this cold gas layer will also be briefly discussed herein.

The results presented here indicate that neither heat conduction or charge exchange could account for the observed loss rates. The losses will probably not be well understood without more detailed experimental observations.

Radial heat conduction. Radial heat conduction losses may be quickly estimated by assuming a constant thermal conductivity. Under this condition, the radial heat conduction equation

$$\rho C_p \frac{\partial T}{\partial t} = \frac{1}{r} \frac{\partial}{\partial r} \left(r K_\perp \frac{\partial T}{\partial r} \right)$$

may be solved analytically. Radial temperature profiles for heat flow in a cylinder are given in Carslaw and Jaeger[4] and are reproduced in

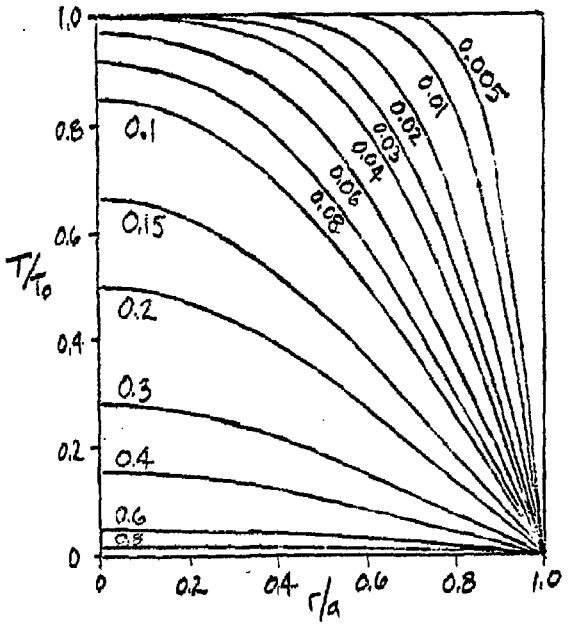

Figure 24. Temperature Distribution at Various Times in a Cylinder of Radius a with Initial Temperature T_o and Zero Surface Temperature. The numbers on the curves are values of $K_\perp t/a^2\rho C_p$ (Ref. 4).

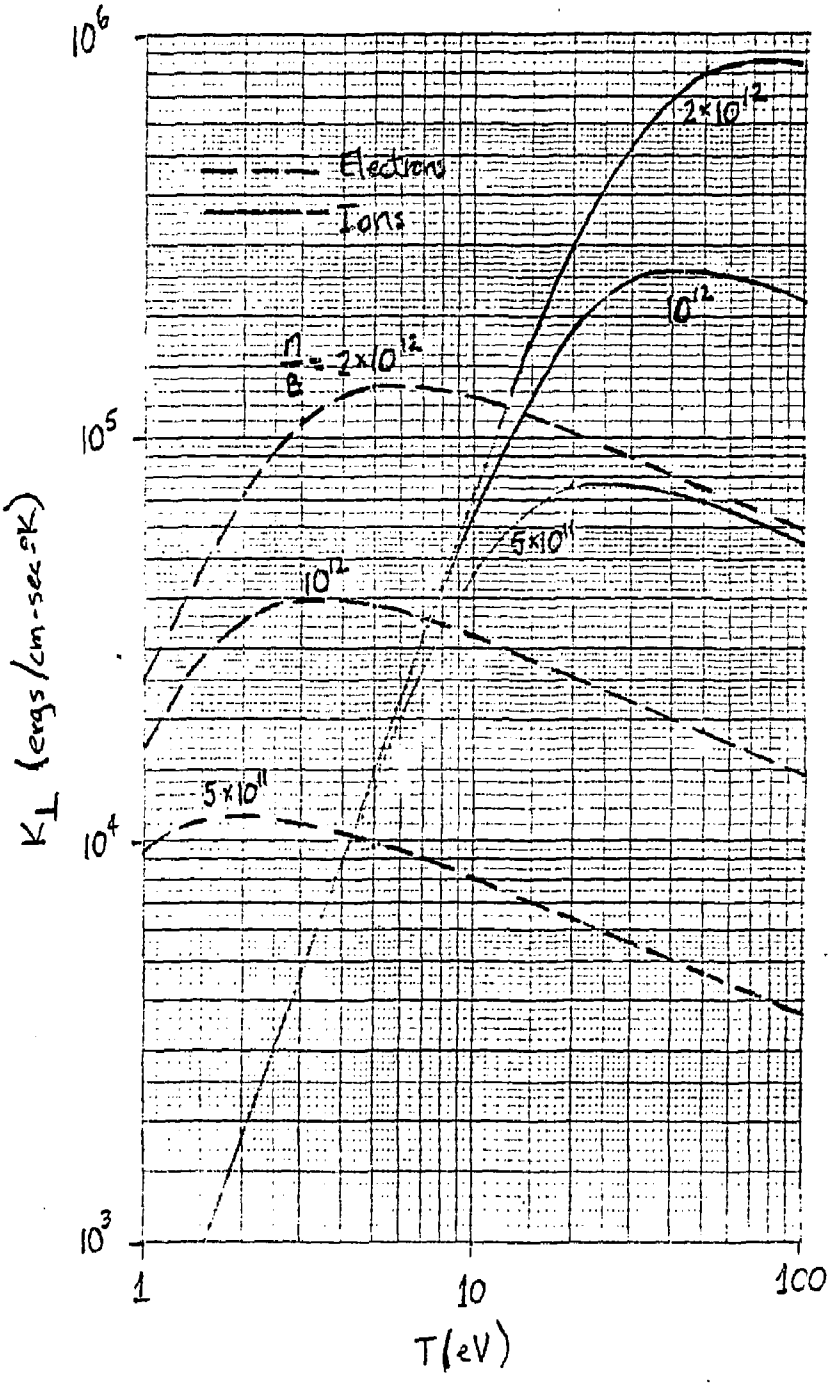

Figure 25. Approximate Cross-Field Thermal Conductivity for a Fully-Ionized Deuterium Plasma. The numbers shown on the curves are values of n/B in $cm^{-3}Gauss^{-1}$. Values of $\ln\Lambda$ were computed based on $n = 3 \times 10^{16} cm^{-3}$.

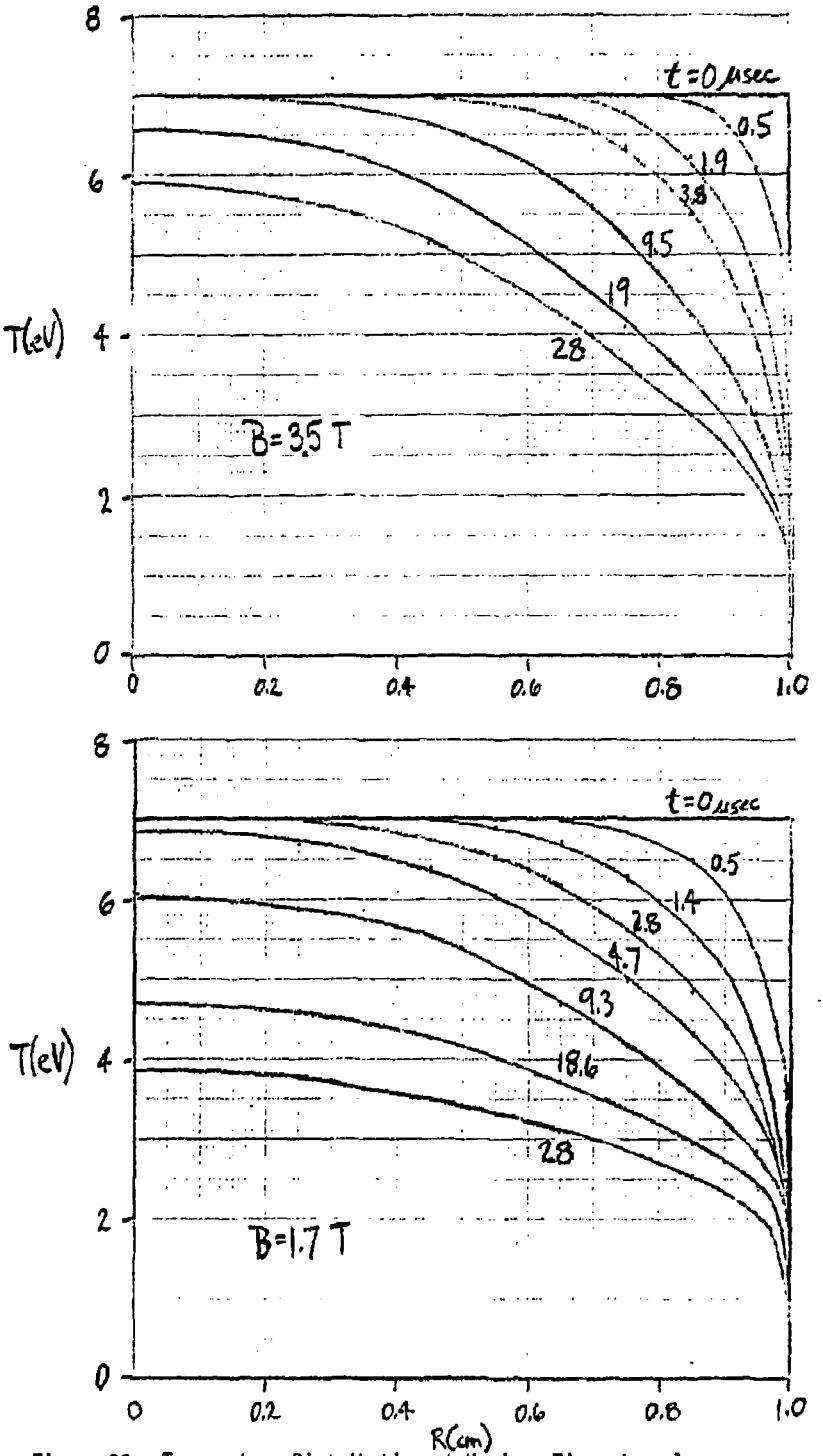

Figure 26. Temperature Distribution at Various Times in a 1-cm Plasma Column with 7 eV Initial Temperature and 1 eV Surface Temperature for $n = 5 \times 10^{15} cm^{-3}$, $Z = 1$ and $A_i = 2$.

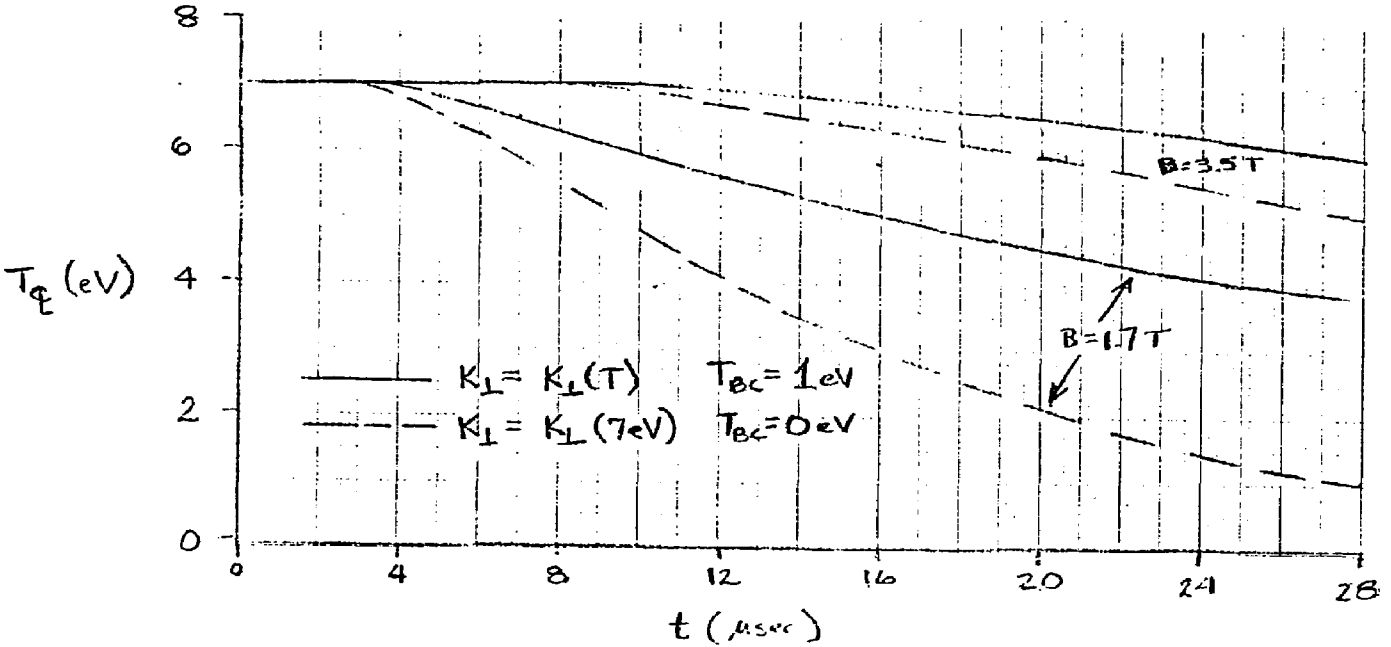

Figure 27. Plasma Temperature at Column Centerline for $n = 5 \times 10^{16} cm^{-3}$, Z = 1, and A_i = 2

Table 1

Typical Parameters of Upgraded Laser-Heated Deuterium Plasma

Assumed Quantities		
Density	n_e	5×10^{16} cm^{-3}
Temperature	$T_e = T_i$	7 eV
Ion Charge	Z	1
Ion Mass	A_i	2
Magnetic Field	B	3.5 Tesla
Radius	r_p	1 cm
Observation Time	τ	2 μsec
Derived Quantities		
Coulomb Logarithm	$\ln\Lambda$	7.2
Cyclotron Frequencies	ω_{ce}	6.2×10^{11} rad/sec
	ω_{ci}	1.69×10^{8} rad/sec
Self-Collision Times	τ_{ee}	1.72×10^{-11} sec
	τ_{ii}	1.04×10^{-9} sec
"Collisionality"	$\omega_{ce}\tau_e$	5.3
	$\omega_{ci}\tau_i$	0.175
Perpendicular Heat Diffusion Time	$\tau_\perp = 0.2\, a^2 \rho C_p / K_\perp$	41 μsec
Equilibration Time	τ_{eq}	0.032 μsec
Mean Free Paths	$\lambda_{ee} = \lambda_{ii}$	0.0033 cm
	λ_o	0.01 cm
Plasma Beta	$\beta = p/(B^2/8\pi)$	0.023

Figure 24. It may be seen that for a cylinder of radius a, uniform initial temperature T_o, and zero edge temperature, the centerline temperature is reduced to $T_o/2$ in a characteristic time

$$\tau_\perp = \frac{0.2\ a^2 \rho C_p}{K_\perp}$$

The approximate parallel thermal conductivity[5,6] for a fully ionized deuterium plasma is plotted in Figure 25. For the conditions of the previous experiment ($n_e = 3 \times 10^{16} cm^{-3}$, $T_e = 7$ eV, and $B = 1.7$ Tesla), we obtain $\tau_\perp = 18$ μsec which is much greater than the observed cooling time of ~2 μsec. For the conditions of the upgraded experiment (see Table 1), $\tau_\perp = 41$ μsec.

As shown in Figure 25 the thermal conductivity in general is not independent of temperature. For typical conditions ($T < 10$ eV, $\frac{n}{B} > 10^{12} cm^{-3}\ G^{-1}$), the cross field conductivity is dominated by the electrons and varies approximately as $T^{5/2}$ for the lower temperatures. Thus, the rate of heat flow is restricted by the cool outer edge of the plasma where the temperature and thermal conductivity are the lowest. Consequently, numerical calculations of the radial heat flow have been completed taking into account the temperature dependence of $K_\perp$. Results are shown in Figure 26 for $n = 5 \times 10^{16} cm^{-3}$ and $B = 1.7$ and 3.5 Tesla. Assumed conditions include a uniform plasma with radius 1 cm, an initial temperature of 7 eV and an edge temperature of 1 eV.

Figure 27 compares the temporal dependence of the plasma temperature at the column centerline for both $B = 1.7$ and $B = 3.5$ Tesla.

It may be seen that increasing the magnetic field should significantly reduce the heat loss. However, the predicted loss rate is about an order of magnitude lower than the observed rate. It may also be seen from Figure 27 that the simple constant thermal conductivity model represents an upper bound on the radial heat loss since, in the region of interest, $K_\perp$ decreases with decreasing T.

Charge exchange with neutral boundary layer. Several investigators have reported studying the behavior of a boundary layer of cool neutral particles interacting with a warm plasma core. Lehnert[7,8] has set forth the conditions under which a plasma is strongly affected by plasma-neutral gas interaction, as well as considering the particle and energy balance of plasmas which are both permeable and impermeable to neutral gas. Oliphant[9-11] has studied the effect of neutral gas in quenching a dense theta-pinch fusion plasma. These studies are in agreement and predict that the presence of a neutral gas layer around a high density plasma has little effect on the particle and energy balance of the central plasma-core.

Lehnert[7] has shown that fast neutrals from charge exchange processes penetrating into a deep plasma layer of constant density and temperature have an e-folding penetration length

$$\lambda_0 = \frac{1}{\sigma_0 n}$$

At increasing plasma temperatures, the effective cross section σ_0 increases rapidly to a maximum σ_{0m} for temperatures on the order of

10 eV after which it slowly decreases with T. For hydrogen $\sigma_{om} \approx 3 \times 10^{-15} cm^2$. Thus, for a characteristic plasma dimension $r_p = 1$ cm there exists a critical density $n_c = 1/\sigma_{om} r_p \approx 3 \times 10^{14} cm^{-3}$ which divides two fundamentally different plasma regimes. When $n \leq n_c$, the plasma is permeable to fast neutrals which penetrate by free streaming. The energy and particle balance is then strongly affected by the wall and boundary layer conditions. On the other hand, if $n >> n_c$, the plasma is impermeable to neutrals provided the temperature is at least of the order of 10 eV. The fully ionized plasma core then becomes separated from the surrounding neutral gas by a thin partially ionized transition layer in which the particle balance is controlled by diffusion.

Since the plasma density is two orders of magnitude greater than the critical density, the LLL experiment is apparently in the latter regime. In this case, analytical and numerical models created by Lehnert[8] and Oliphant[9-11] show that the plasma energy losses are controlled by radial heat conduction across the plasma and boundary layer. Thus, the presence of the neutral boundary layer should not result in significantly higher energy loss rates than estimated by classical radial conduction. Thus, the presence of a neutral boundary layer should have little effect on the energy balance of a high density plasma in contact with the wall.

APPENDIX

NOMINAL 100 eV PLASMA SOURCE

In order to achieve a 100 eV plasma through CO_2 laser heating, it will be necessary to operate at 3 to 10 x 10^{17} cm^{-3} electron densities. At the corresponding neutral gas fill densities, the laser intensity alone is sufficient to break down the gas, and two methods of operation become feasible. A theta-pinch plasma can be formed, but low inductance circuitry is required to create a necessary beam trapping density minimum. Conversely, the gas can be puff-filled into a plasma tube and a breakdown wave propagated down the tube. We have demonstrated both techniques and propose a device to do the latter, but to also be capable of performing the former task.

A constant density bleaching wave produces a temperature profile of

$$T = T_0\left[\left(\frac{5}{2}\int_0^{\tau} \tilde{I}\, d\tau'\right)^{3/5} - \frac{3}{2}y\right]^{2/3}$$

where $\tau = t/t_0$, $\tilde{I} = It_0/E_0$, $y = x/\ell_0$, t_0 is the laser pulse time, and E_0 is the laser energy fluence. The characteristic temperature and absorption lengths are

$$T_0 = \frac{E_0}{2n_0 c_v \ell_0} = 132[E_0(kj/cm^2)\bar{n}_0(10^{18}\ cm^{-3})]^{2/5}\ eV$$

and

$$\ell_0 = \frac{0.01\ T_0(eV)^{3/2}}{\bar{n}_0^{\,2}(10^{18}\ cm^{-3})} = 15.2\ \frac{E_0^{3/5}\ (kj/cm^2)}{\bar{n}_0^{\,2/5}(10^{16}\ cm^{-3})}\ cm$$

At the plasma column midpoint, $\ell_0/2$, the temperature will equal T_0 at the end of the laser pulse.

We have chosen the following nominal design points based on the above scaling and available experiment equipment:

$$T_0 = 100 \text{ eV}$$

$$n_0 = 0.7 \times 10^{18} \text{ cm}^{-3} \text{ (10 torr fill pressure)}$$

$$\ell_0 = 20 \text{ cm}$$

$$\varepsilon_0 = 700 \text{ joules}$$

$$A_0 = 1 \text{ cm}^2$$

$$t_0 = 2 \text{ μsec}$$

Our large laser heated solenoid facility has been operated at just such conditions. Plasma columns well over 20-cm long have been produced and, from both luminosity and diamagnetic loop measurements, appear to uniformly fill the plasma tube, even though the laser energy is admitted through a small mm-sized hole at one end. The characteristic acoustic flow speed of 10 cm/μsec would restrict the test time, except that the small hole (plus a slightly larger hole at the far end to admit the gas) will cut down the end flow significantly. The dominant loss mechanism will then be parallel electron heat conduction and radial heat conduction. The latter can be restricted by a strong axial magnetic field. The following quantities are useful to evaluate these loss mechanisms.

$$\omega_{ce}\tau_e = 4B(T)$$

$$\omega_{ci}\tau_i = 0.14\ B(T)$$

$$D_{\perp e} = 10 \text{ cm}^2/\text{μsec}$$

$$\tau_{\parallel e} = \frac{(\ell/2)^2}{D_{\parallel e}} = 10\ \mu\text{sec}$$

$$\tau_{ei} = 0.1\ \mu\text{sec}$$

$$D_{\perp i} = 17/B^2(T)\ \text{cm}^2/\mu\text{sec}$$

$$\tau_{\perp i} = \frac{a^2}{D_{\perp i}} = 0.02\ B^2(T)\ \mu\text{sec}$$

Radial heat conduction is seen to be the most significant loss mechanism, and 10 T or higher magnetic fields are required to provide 2 μsec of test time. In order to provide good optical access and reasonable field uniformity between split coils, we propose using (2) 10-cm long, 8 turn, 4-cm ID solenoids. These solenoids will require about 10 kJ to produce 10 T. This could conceivably be accomplished with the present 20 kV capacitor bank, but there would then be no possibility of operating in the theta-pinch mode, or of possibly lifting the plasma off the wall to restrict radial heat conduction. We propose using a present low inductance fast capacitor bank which, with the purchase of (12) capacitors, could supply 40 kJ at 50 kV.

The cold cathode CO_2 laser would be operated in its normal unstable resonator configuration. The present laser can only produce about 350 joules, and we would be restricted to about 70 eV temperatures at somewhat lower densities. The material cost and labor times for modifying the present equipment, upgrading the capacitor bank, and upgrading the laser are listed below.

	Material Costs	Labor Time	Cost w/Overhead
1. Experiment Modification	$5,000	5 person-months	$12,500
2. Capacitor Bank Upgrade	$9,000	2 person-months	$ 5,000
3. Laser Upgrade to 15 cm Optics (700 joules)	$31,000	3 person-months	$ 7,500
Total	$45,000	10 person-months	$25,000

The pacing item would be the experimental modification, which would take approximately three months. A senior scientist would be needed about 1/3 time to supervise the work. The total loaded costs would be about $100,000. This only includes the most basic shakedown of the system.

REFERENCES

1. E.A. Crawford et al., "Measurement of Plasma Cooling Rate Due to Impurity Radiation in the Laser Heated Plasma Sample Facility," MSNW Report 77-1058-1 (1977).

2. G. Becker and D.F. Düchs, "Plasma Transport Computations for High-Beta Plasmas with Impurities and Neutrals," Nuc. Fus. 16, 5 (1976).

3. A.W. DeSilva and R.E. Pechacek, "Use of Varistors to Produce Single High-Current Pulses," Rev. Sci. Instrum. 47, 431 (1976).

4. H.E. Carslaw and J.C. Jaeger, Conduction of Heat in Solids, Oxford University Press (1959).

5. L. Spitzer, Physics of Fully Ionized Gases, 2nd Ed. Interscience (1962).

6. S.I. Braginskii, "Transport Processes in a Plasma," in Reviews of Plasma Physics, Vol. I, M.A. Leontovich, Editor, Consultants Bureau Enterprises (1965).

7. B. Lehnert, "Relaxation Times of Permeable Plasmas," Plasma Physics 17, 689 (1975).

8. B. Lehnert, "Screening of a High-Density Plasma from Neutral Gas Penetration," Nuc. Fus. 8, 173 (1968).

9. T.A. Oliphant et al., "Transient Charge-Exchange Effects in a Neutral-Gas Layer," Nuc. Fus. 16, 263 (1976).

10. T.A. Oliphant, "Heat Transfer Through a Reference Theta-Pinch Reactor (RTPR) Cooling Layer," in Proceedings of the First Topical Conference in the Technology of Controlled Nuclear Fusion (1974) p. 667.

11. T.A. Oliphant, "Plasma Cooling of a Pulsed Thermonuclear Reactor by Means of a Neutral Gas Layer," Nuc. Fus. 13, 521 (1973).